İSTANBUL TECHNICAL UNIVERSITY ★ GRADUATE SCHOOL OF SCIENCE ENGINEERING AND TECHNOLOGY

SCOUR AND FLOW AROUND PILE SUPPORTED WHARF UNDER WAVES

M.Sc. THESIS

Dila DEMİRAL

Department of Civil Engineering

Hydraulics and Water Resources Engineering Programme

JUNE 2016

İSTANBUL TECHNICAL UNIVERSITY ★ GRADUATE SCHOOL OF SCIENCE ENGINEERING AND TECHNOLOGY

SCOUR AND FLOW AROUND PILE SUPPORTED WHARF UNDER WAVES

M.Sc. THESIS

Dila DEMİRAL
(501141503)

Department of Civil Engineering

Hydraulics and Water Resources Engineering Programme

Thesis Advisor: Prof. Dr. Şevket ÇOKGÖR

JUNE 2016

İSTANBUL TEKNİK ÜNİVERSİTESİ ★ FEN BİLİMLERİ ENSTİTÜSÜ

DALGA ETKİSİ ALTINDA KAZIK VE PALPLANŞ ÇEVRESİNDE AKIM VE OYULMA

YÜKSEK LİSANS TEZİ

Dila DEMİRAL
(501141503)

İnşaat Mühendisliği Anabilim Dalı

Hidrolik ve Su Kaynakları Mühendisliği Programı

Tez Danışmanı: Prof. Dr. Şevket ÇOKGÖR

HAZİRAN 2016

Dila Demiral, a M.Sc. student of İTU Graduate School of Science Engineering and Technology student ID 501141503, successfully defended the thesis entitled "SCOUR AND FLOW AROUND PILE SUPPORTED WHARF UNDER WAVES", which she prepared after fulfilling the requirements specified in the associated legislations, before the jury whose signatures are below.

Thesis Advisor :	**Prof. Dr. Şevket ÇOKGÖR** İstanbul Technical University	.....
Jury Members :	**Assoc. Prof. Dr. V. Ş. Özgür KIRCA** İstanbul Technical University	.....
	Assoc. Prof. Dr. Yeşim ÇELİKOĞLU Yıldız Technical University	.....

Date of Submission : 2 May 2016
Date of Defense : 8 June 2016

To my family,

FOREWORD

This thesis is written during my postgraduate education at İstanbul Technical University in the dates between September 2015 and May 2016. When I was studying on this thesis; I have received help from a lot of valuable people. To begin with, I would like to thank my advisor Prof. Dr. Şevket Çokgör for guiding me the best way he can, giving me a lot of valuable advices and not to refrain to support. I want also to thank Assoc. Prof. Dr. Oral Yağcı and Assoc. Prof. Dr. V. Ş. Özgür Kırca for their help, support and precious advices. Another important person I cannot pass without thanking is Işılsu Yıldırım. She has always been my source of motivation since we met. She has become one of my best friends. And all this time, she has always been supportive and helpful. Best friends are always there for you. I think I am very lucky to have a lot of good friends like Akif, Bilgen, Gizem, Göksel, Engin, Halil, Onuralp and Ufuk. Their presence is too valuable for me. In addition, I want to thank Research Assistant Mehmet Furkan Çelik for his great effort to make time for helping me over my experiments. Besides, I would be glad to thank Hasan Yalçın, Mevlüt Uluçınar and Yaşar Aktaş for helping me on all my experiments. I also would like to thank TÜBİTAK (The Scientific and Technological Research Council of Turkey) that supported me financially during my postgraduate education with the National Scholarship Programme for M.Sc. Students.

Lastly, I want to thank my family. This thesis would not be written without my mother's and father's unrequited love and emotional support. I am the youngest member of my family, and I know that I am so lucky to have two sisters like Sena and Serra who always treat me like I am their little princess. And I want also to thank them to give me two brothers, Barış and Resai, who are always kind and supportive. And I would like to give my special thanks to my two little nephews, Ateş and Efe, also to my cousin Umutcan for being in my life and cheering me up all the time when I needed.

May 2016

Dila DEMİRAL
(Civil Engineer)

TABLE OF CONTENTS

Page

ABBREVIATIONS

ADV **:** Acoustic Doppler Velocimeter

SYMBOLS

a	: Amplitude of the horizontal component of orbital motion of water particles
a_s	: Amplitude of the horizontal component of water-particle motion at the sea surface
B	: Flume width
C_D	: Drag coefficient
C_M	: Inertia coefficient
C_m	: Hydrodynamic mass coefficient
c_g	: Group velocity
D	: Pipe/pile diameter
d	: Grain size
d_{50}	: Grain size
F	: Force acting per unit length of the cylinder on the structure in the inline direction
F_p	: Froude-Krylov force
f_w	: Wave boundary layer friction coefficient
g	: Acceleration of gravity
H	: Wave height
KC	: Keulegan-Carpenter number
KC_s	: Keulegan-Carpenter number at the sea surface
k	: Wavenumber
k_N	: Equivalent sand roughness of the bed
L	: Wavelength
L_0	: Deep-water wavelength
m'	: Hydrodynamic mass
U	: Flow velocity
u	: Maximum near bed velocity of wave induced orbital currents resp. mean velocity in case of steady currents
U_c	: Undisturbed near-bed current velocity
u_c	: Critical velocity for beginning of sediment motion
U_f	: Bed shear velocity
U_{fm}	: Maximum value of bed shear velocity in waves
U_m	: Maximum value of undisturbed orbital velocity at the bed
U_r, U_θ	: Plan view components of undisturbed orbital velocity at the bed
P	: Wave power
p	: Mean pressure
p_0	: Hydrostatic pressure
Re	: Reynolds number
S	: Scour depth
s	: Specific gravity of sediment grains
T	: Wave period

$\boldsymbol{t}$: Time
$\boldsymbol{z}$: Depth measured from the bottom
$\boldsymbol{\theta}$: Shields parameter
$\boldsymbol{\theta_{cr}}$: Critical shields parameter
$\boldsymbol{\nu}$: Kinematic viscosity
$\boldsymbol{\rho}$: Water density
$\boldsymbol{\sigma}$: Geometric mean
$\boldsymbol{\tau_{\infty}}$: Undisturbed bed shear stress in current

LIST OF FIGURES

Page

SCOUR AND FLOW AROUND PILE SUPPORTED WHARF UNDER WAVES

SUMMARY

The design of large marine structures are essential because of their large application fields, such as bridge piers, offshore gravity platforms and pile supported backfilling zones. In order to design these types of marine structures, the flow mechanism around the structures must be well understood and analyzed. Since the flow around the structure will cause an increment of the local sediment transport, eventually it will cause scour formation around the structure. The structures built in a marine environment are exposed to waves, currents, or combination of them. However, in the marine environment waves are generally more dominant than currents. The current induced scour and wave induced scour have different mechanisms; therefore they must be investigated separately.

Pile supported reclamation zones can be built as a pile row. Piles are attached to each other or with a gap, which fills with sheet between the pile surfaces. The surcharge and wave loads acting on the structure must be analyzed properly, especially when the erodible bottom condition is valid, since scour can be a great threat to the structural stability. In this study, in order to understand the flow mechanism and scour process around pile-supported wharfs, a series of experiments were conducted in İstanbul Technical University Hydraulics Laboratory. Experiments were held in a regular wave flume, which is 22.5 m in length, 1 m in width and 0.5 m in height. Two twin cylinders, which has 22.5 cm diameter, were used as experimental model. They were flush mounted to the flume wall and flume base. First of all, rigid bed experiments were conducted. Secondly, actual erodible bed experiments were made for different gap ratios. In all the experiments, wave conditions were the same and water depth was 34.5 cm. Pressure measurements, velocity measurements and bottom scanning were made for all the tests in order to get a better understanding of the flow mechanism around the cylinder(s). Pressure measurements were made with five transducers which are located 5 cm above the bed and placed on the surface of the cylinder with 45° intervals. Velocity measurements were made at the undisturbed bed with an Acoustic Doppler Velocimeter (Vectrino). The bottom was scanned before and after the experiments in order to determine the scour and deposition depths around the structure. In all the tests, the maximum scour depth was seen at the incoming wave side, between the flume wall and cylinder. In this zone, vortex formation was observed and it was the cause of scour. However, the scour around the cylinder except this region was independent from the vortex generation. The scour around the cylinder was because of the wave induced steady streaming mechanism. The results of the experiments indicated that, where x is the distance between the cylinders and D is the pile diameter, the most critical case of scour depth was observed in the cases of $x/D = 1.5$ for steady streaming zone. For this test, the maximum scour depth to the cylinder diameter ratio, was $S/D = 0.09 \sim 0.13$. The results also showed that there is a relation between the pore pressure and deposition.

DALGA ETKİSİ ALTINDA KAZIK VE PALPLANŞ ÇEVRESİNDE AKIM VE OYULMA

ÖZET

Köprü ayakları, açıkdeniz ağırlık platformları, kazık destekli dolgu limanlar, a.ık deniz rüzgar türbinleri gibi kullanım alanı çok geniş olan büyük deniz yapılarının öneminin artmasıyla beraber, bu yapıların tasarım ve projelendirilmesinin düzgün yapılabilmesi de büyük önem kazanmıştır. Bu tür yapıların tasarımının güvenli ve ekonomik olması için yapının etrafındaki akım alanının iyi analiz edilmesi gerekir. Çünkü deniz ortamına inşa edilen yapı, çevresindeki akımı değiştirecektir ve bu değişim bölgesel sediment hareketini arttırarak sonunda yapı çevresinde oyulmaya sebep olacaktır. Bu oyulma yapının stabilitesine zarar verebilir. Deniz yapıları akıma, dalgaya ya da bu iki mekanizmanın birleşimine maruz kalabilirler. Ancak deniz ortamında dalga etkisi akım etkisinden daha baskındır. Akımın ve dalganın sebep olacağı oyulma mekanizmaları birbirinden farklı olacağı için bu durumlar birbirinden ayrı incelenmelidir.

Kazık temelli dolgu limanlarda ve rıhtımlarda kazıklara etkiyen sürşarj yükü, gemi yanaşmalarından dolayı etki edecek yükler ve su yüklerinin doğru tahmin edilmesi, özellikle taban oyulmaya müsaitse büyük önem taşır. Çünkü yapının tabanında meydana gelebilecek oyulma, yapının stabilitesine zarar vererek yapının hasar görmesine hatta yapının yıkılmasına yol açabilir.

Bu çalışmada, kazık destekli rıhtımların kazıklarına etkiyecek kuvvetlerin bulunabilmesi, yapı etrafındaki akım mekanizmasının ve meydana gelecek oyulmanın sebep ve yerinin anlaşılabilmesi için, İstanbul Teknik Üniversitesi Hidrolik Laboratuvarı'nda deneysel bir çalışma yapılmıştır. Deneyler 22.5 m uzunluğunda, 1 m genişliğinde ve 0.5 m derinliğindeki düzenli dalga kanalında yürütülmüştür. Tek silindir durumu için ve farklı açıklıklarla yerleştirilen iki silindir ile yapılan deneylerde, silindirlerin çapı aynıdır ve 22.5 cm'dir. Silindirlerden birinin cidarında basınç ölçümü yapılmış ancak diğer silindirde ölçüm yapılmamıştır. Kullanılan silindirdirler PVC'dir ve bu silindirlerin yüzeyi hidrolik olarak pürüzsüzdür. Silindirler hem tabana hem de kanal duvarına bitişik şekilde dikey olarak yerleştirilmiştir. Bu sayede silindir ve kanal duvarının ve kanal tabanının birleştiği yerlerde su ve sediment geçişi engellenmiştir. x, silindirlerin merkezleri arasındaki uzaklık ve D silindir çapı olmak üzere x/D sırasıyla 2, 1.5 ve 1 için deneyler yapılmıştır. Bu konfigürasyonlarda ölçüm yapılmayan silindir hem dalga geliş yönüne hem de mansap yönüne yerleştirilmiştir. Deneyler hem sedimentsiz (rijit) tabanda hem de oyulma desenini gözlemleyebilmek için sedimentli tabanda yapılmıştır. Sedimentli deneylerde kanal tabanına 3 m uzunlukta, 1 m genişlikte ve 6 cm yüksekliğinde bir sediment havuzu yerleştirilmiştir. Bu deneylerde kullanılan yatak malzemesinin ortalama çapı 0.72 mm'dir. Deneyler aynı dalga koşullarında yapılmıştır, su derinliği tüm deneylerde 34.5 cm'dir. Dalga boyu 1.15 m, dalga yüksekliği 0.13 m ve dalga periyodu 0.9 saniyedir. Keulegan Carpenter sayısı yaklaşık 1'dir. Hesaplanan Shields parametresi kritik Shields parametresinden

büyüktürö yani tüm deneylerde taban hareketlidir. Bu sebeple oyulma deneylerinde kanal duvarı ile yapı arasında oluşan oyulma çukurunun deney süresinde tekrar dolduğu ve oyulduğu gözlemlenmiştir.

Yürütülen deneylerde silindir cidarında aynı seviyedeki beş farklı noktada basınç ölçümü ve yapının 4 m uzağındaki bir noktada hız ölçümü yapılmıştır. Basınç ölçümleri tabandan 5 cm yukarıda, silindir cidarına 45° açıyla yerleştirilen 5 adet Mesens tipi basınç dönüştürücüsü ile yapılmıştır. Hız ölçümleri, tabandan 5 cm yukarıda, akustik Doppler hızölçer (Vectrino I) kullanılarak yapılmıştır. Ölçülen hızlar ve hesaplanan hızlar karşılaştırıldığında değerlerin birbirine benzer olduğu gözlemlenmiştir.

Her deney sonrasında kanaldan su boşaltılırken yatak formunun korunabilmesi için sedimentli tabanın altına yapının etkilenmeyeceği şekilde drenaj boruları yerleştirilmiş ve su yavaş bir şekilde boşaltılmıştır. Oyulma derinliğinin ve birikme miktarının saptanabilmesi için sedimentli durumda kanal tabanı deney öncesinde ve deney sonrasında bir lazer tarayıcı (Leica Laser Scanner) ile taranmıştır. Lazer tarayıcıyla elde edilen sonuçlar hem görselleştirilmiş hem de eş derinlik eğrisi haritaları çıkarılmıştır. Böylece yapı etrafındaki oyulma ve birikme desenlerinin oluştuğu yerler detaylı olarak görülebilmiştir. Deneylerin her biri 6 saat yapılmıştır. Bu süre boyunca deneyler aralıklı olarak kamerayla kaydedilmiş ve yapı çevresinde oluşacak akım mekanizması ve oyulmanın nerede olduğu gözlemlenmiştir.

Elde edilen deney sonuçlarına göre dalganın geliş yönünde, silindir ve kanal duvarının bitişik olduğu bölgede yapı geniş kazık kategorisine girmesine ragmen ($D/L > 0.1$) atnalı çevrintilerine benzer çevrintilerin oluştuğu görülmüştür (D silindir çapı, L dalga boyudur). Bu çevrintiler kamerayla kaydedilmiş ve yavaşlatılarak izlenmiştir. Oluşan çevrintinin periyodu ile dalga periyodunun birbirine yakın olduğu gözlemlenmiştir. Bu çevrintilerin periyodu 0.8 saniye civarindadir. Yapı ve dalga kanalının birleştiği yerde gelen dalga yönünde meydana gelen oyulmaya burada oluşan çevrintilerin sebep olduğu saptanmıştır. Deney konfigürasyonu değişmesine rağmen tüm deneylerde, bu bölgedeki oyulma derinliklerinin birbirine yakın olduğu görülmüştür. Ancak gözlenen en büyük oyulmanın $S/D = 0.18$ olduğu saptanmıştır (S, oyulma derinliği). Test sonuçlarına göre tüm deneylerde gözlemlenen en fazla oyulmanın gelen dalga yönünde silindir ve kanal duvarı arasında meydana geldiği görülmüştür. Ancak oyulma sadece bu bölgeyle sınırlı değildir. Silindirlerin etrafında meydana gelen oyulmanın, zamansal ortalama akıntılar sebebiyle oluştuğu gözlemlenmiştir. Sedimentli tabanın final durumundaki topografyası lazer tarayıcı ile çıkarılmış ve oluşan desenler incelenmiştir. Görseller incelendiğinde, oyulma desenlerinin zamansal ortalama akıntılar sebebiyle oluştuğu fikri desteklenmiştir. Tüm deneyler için akıntı gözleri ve bunların etki alanları çıkarılmış, meydana gelen oyulma ve birikmeler eş derinlik haritalarıyla şematize edilmiştir. Akıntı gözlerinin oluştuğu bölgede meydana gelen en büyük oyulmanın $x/D = 1.5$ konfigürasyonunda olduğu gözlemlenmiştir. Bu durumda $S/D = 0.09{\sim}0.13$ olarak kaydedilmiştir. Sumer (2001) ve Khalfin (2007) benzer deney koşullarında geniş kazık durumunda oyulma desenlerini incelemişlerdir. Bu çalışmalar incelendiğinde Sumer (2001), boyutsuz oyulma derinliğinin yapı yakınında en fazla $S/D = 0.04$ olarak, Khalfin (2007) $S/D = 0.07{\sim}0.08$ olarak bulmuştur. Bu araştırmacıların bulguları ve yapılan çalışma karşılaştırıldığında boyutsuz oyulma derinliğinin daha fazla olduğu görülmektedir. Bu durumun sebebi deney sınır koşullarının farklılığıdır. Akıntı gözlerinin oluştuğu bölgede oyulmanın en düşük olduğu durum $x/D = 1$ durumudur. $x/D = 2$

durumlarında akıntı gözleri bölgesinde oluşan oyulmanın tek silindir durumunda meydana gelen oyulma ile benzerlik gösterdiği görülmüştür. Silindirler arasındaki uzaklık daha fazla açıldıkça yapı artık tek silindir gibi davranacaktır.

Deney sonuçları ayrıca tabanda meydana gelen birikmenin ve oyulmanın, sırasıyla bu bölgede ölçülen basınçta değişim yarattığını göstermiştir. Tabanda birikme meydana geldiğinde ölçülen basıncın azaldığı, taban oyuldukça bu noktada ölçülen basıncın arttığı gözlemlenmiş ve bir grafikte gösterilmiştir.

1. INTRODUCTION

1.1 Definition of Problem

In recent years, the marine structures, which have a great role in water transportation, became more significant. Hence, it is an essential concern for engineers to design these structures properly; the design must be safe and economical.

The structures built in marine environment are widely exposed to currents, waves or combined waves and currents. In marine environment, waves are more dominant than currents. Since the presence of these bodies will change the flow pattern in the vicinity of the structure, the interaction between the structures and flow must be analyzed properly in order to make a proper design. Especially scour around a large marine structure under waves is an important subject that must be examined because of its application in many projects, such as bridge piers, offshore gravity platforms, platform legs and pile supported backfilling ports.

Pile supported backfilling ports are used commonly, such as container terminals that need a large storage area. The most crucial members of these ports are piles. Pile supported reclamations can be built as a pile row that piles are attached to each other or with a gap, which fills with sheet between the pile surfaces. These pile supported wharfs built in marine environment have to be well designed and preserved against the waves, surcharge loads, lateral loads due to the earth push and ship berting, especially when the bottom is erodible. In order to design these types of structures safely against scour, the flow mechanism around the structures must be analyzed properly. Because scour around the piles or pile groups could be a threat to the stability of the structure in erodible bottom case.

In the present study, in order to clarify the scour mechanism and obtain the forces acting on the pile-supported wharfs, the pile supported wharf was modelled and studied experimentally in a laboratory wave flume. Scour process and flow mechanism around the pile(s) were investigated by flow visualization, monitoring erodible bed and pressure measurements on the surface of the pile.

1.2 Scope of Study

This experimental study was made in order to determine the scour characteristics and flow mechanism around the pile-supported wharfs. In this context, the explanations of the related subjects were made in the literature review part.

Firstly, hydrodynamics around the cylindrical structures was presented, namely the forces acting on the body were explained in details. Secondly, the scour mechanism for slender pile regimes and large pile regimes are given, the difference between these mechanisms was explained. In the third part of this thesis, experimental setup and the conducted experiments were represented in details. The experimental facilities, measurement devices and test conditions were explained. The fourth part of the thesis is about the experimental results. In this section, the results of tests were evaluated and also presented in graphics, definition sketches and maps. The fifth and last section focused on the conclusion and recommendations. This part of study includes the brief results of experiments and gives some suggestions about the problems related within this study.

2. LITERATURE REVIEW

2.1 Hydrodynamics Around Cylindrical Structures

In recent years, rapid growth in construction of marine structures raised the importance of the knowledge of interaction between the structure and its surrounding area. For engineering fields, it is significant to understand the mechanism of flow around a marine structure. When the structure is in steady current regime, the hydrodynamic quantities that characterise the flow mainly depend on the Reynolds number (Re). Where, U is the flow velocity, D is the cylinder diameter and ν is the kinematic viscosity, Re is defined as:

$$Re = \frac{UD}{\nu} \tag{2.1}$$

However, in the case of waves, an additional parameter, which is called as Keulegan Carpenter (KC) number appears (Sumer and Fredsøe, 1997). In this present study, flow around a circular cylinder in waves will be explained since that case is considered on this thesis. Flow around a circular cylinder is a subject, which must be investigated as a subtopic of hydrodynamics. Once the flow mechanism is clarified, the forces acting on the body can be determined. It is important to ascertain the exact forces acting on the structure for the stability and performance. The books written by Sarpkaya and Isaacson (1981) and Sumer and Fredsøe (1997) are about the hydrodynamics around the structures. Sarpkaya and Isaacson (1981) concentrated on both diffraction regime and drag dominated regime, while Sumer and Fredsøe (1997) primarily focused on drag-dominated regime. Sumer and Fredsøe (1997) indicated that, flow separation; vortex shedding and turbulence have a great effect in the drag-dominated regime.

2.1.1 In-line force in oscillatory flow

When a cylindrical structure is exposed to waves, it is subjected to two kinds of forces, namely the in line force and lift force (Figure 2.1).

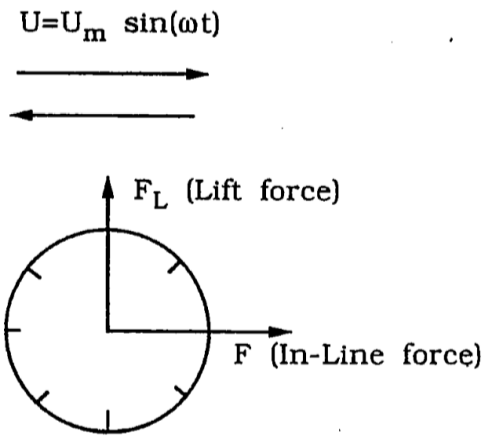

Figure 2.1 : Definition sketch (Sumer and Fredsøe, 1997, p. 124).

For the case of oscillatory flow, the force acting per unit length of the cylinder on the structure in the inline direction is given by the following formula

$$F = \frac{1}{2}\rho C_D D U|U| + m'\dot{U} + \rho A\dot{U} \tag{2.2}$$

Herein, C_D is the drag coefficient, $m'\dot{U}$ is hydrodynamic mass force and $\rho A\dot{U}$ is Froude-Krylov force. Hydrodynamic mass force is the force acting on the body, when the body is moved with an a acceleration and it creates a pressure gradient around the body. This effect causes the acceleration of the fluid in the immediate neighborhood of the structure. In equation 2.2, m' is hydrodynamic mass, which can be expressed as $m' = C_m \rho A$ and A is the volume per unit length of the cylinder. Therefore, equation 2.2 can be re-written as:

$$F = \frac{1}{2}\rho C_D D U|U| + \rho(C_m + 1)A\dot{U} \tag{2.3}$$

Where $C_m + 1 = C_M$ and C_M is the inertia coefficient.

$$C_D, C_M = f(KC, Re) \tag{2.4}$$

KC is the Keulegan-Carpenter number and it is given by the following formula:

$$KC = \frac{U_m T}{D} \tag{2.5}$$

Herein, U_m is the maximum orbital wave velocity, T is the wave period and D is the cylinder diameter.

When the body is fixed and the fluid is moved with an a acceleration, two reactions are observed. Firstly, hydrodynamic mass is generated. Secondly, the accelerated fluid will cause a pressure gradient generation in the outer flow region, which can be shown as:

$$\frac{\partial p}{\partial x} = -\rho \frac{dU}{dt} \tag{2.6}$$

In which, U is the velocity in the outer region. The pressure gradient that is calculated by the equation 2.6 will produce the force, which is called as Froude-Krylov force. This force is calculated by:

$$F_p = -\oint_S p ds \tag{2.7}$$

In here, S is the surface of the cylinder (Sumer and Fredsøe, 1997).

2.1.2 Lift force in oscillatory flow

When a structure is under the oscillatory flow effect, it can be exposed to the lift force, as can be seen in Figure 2.1. For oscillatory flow, the parameter KC appears, as mentioned in the preceding paragraphs. This KC number is given by the equation 2.5. As will be detailed later, if the Keulegan-Carpenter number has small values, the flow around the cylinder is in the unseperated flow regime. Hence, there will be no lift force generation in this situation (Sumer and Fredsøe, 1997).

2.2 Scour in the Marine Environment

When a structure is built in marine environment, it will change the flow pattern in the vicinity of the structure. Therefore, there will be a flow contraction, horseshoe vortex generation in front of the structure, lee wake vortices formation behind the structure, turbulence generation, wave reflection and diffraction, wave breaking and pressure differentiation in the soil (Sumer and Fredsøe, 2002). These facts will have a great effect on the local sediment transport. As a result, the scour will occur. Scour can be classified as clear water scour and live bed scour. There is no sediment motion away from the structure in the clear water scour, namely $\theta < \theta_{cr}$ (Figure 2.2). In the live

bed scour, there is sediment motion all over the bed, $\theta > \theta_{cr}$ (Sumer and Fredsøe, 2002). Here θ is the Shields parameter and it is calculated as follows:

$$\theta = \frac{U_f^2}{gd(s-1)} \tag{2.8}$$

Here, g is the acceleration of gravity, d is the grain size, s is the specific gravity of sediment grains, U_f is the undisturbed shear velocity and defined as $U_f = \sqrt{\tau_\infty/\rho}$. Here, τ_∞ is the maximum value of undisturbed bed shear velocity and ρ is the specific mass of the water.

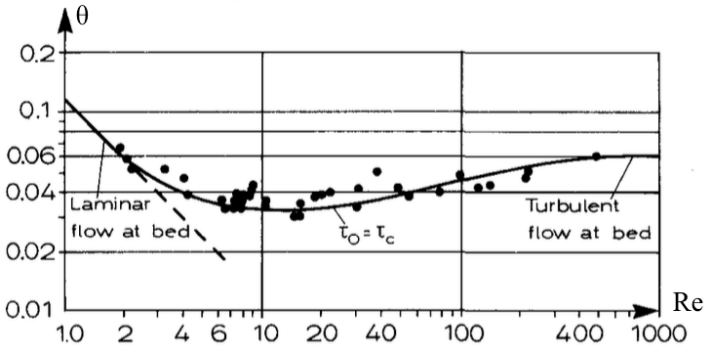

Figure 2.2 : The Shields diagram giving the threshold value θ_{cr} as a function of $Re = U_f d/\nu$ (Fredsøe and Deigaard, 1992, p. 203).

Both in clear water and live bed scour case, scour can be a threat to the structure stability, for example, it can cause of bridge failure. Scour can occur around several types of structures, such as bridge piers, pipelines, piles, breakwaters, and seawalls. These structures are generally exposed to currents, waves or combined waves and currents. In the marine environment, waves are more dominant than currents. Since there are two kinds of flow regimes around a pile in marine environment under waves, there will be two kinds of scour process: scour around a slender pile and scour around a large pile (Sumer and Fredsøe, 2002).

2.3 Scour in Slender Pile Regime

In river environment, scour around bridge piers is one of the most important reasons of bridge failure. According to National Bridge Inventory (1997), 500.000 of 600.000 bridges in the United States are over water. Briaud et al. (1999) indicated that 1000 of these 600.000 bridges have collapsed between the years of 1970 and 1999, 60% of those failures were because of scour.

When a vertical circular pile is placed in marine environment, it will change the flow pattern in the neighbourhood. If the pile size is too small when it is compared to the wavelength $(D/L < 0.1)$, the presence of the pile does not influence the wave. Therefore, separation vortices are observed. This regime is called as slender pile regime. In this regime, there will be horseshoe vortex generation in front of the pile and lee wake vortices formation at the lee-side of the pile. Moreover, due to the flow deceleration in front of the pile, downflow mechanism is observed. The downflow, horseshoe vortex and lee-wake vortices have an effect of increment on the local sediment transport around the structure, thus lead to scour if the bed is erodible (Sumer and Fredsøe, 2002).

Horseshoe vortex is generated at the bed due to the rotation of incoming flow velocity. Since the rotation in the flow and the adverse pressure gradient caused by the presence of the structure, the bed boundary layer on the upstream side of the pile goes through a three dimensional separation (Figure 2.3). This separated boundary layer turns into a spiral vortex form around the structure, and then weakens at downstream side. Two conditions must be prevailed for horseshoe vortex generation. First of all, there must be an incoming boundary layer with a thickness of δ. Secondly, the adverse pressure gradient generated by the presence of the pile must be strong enough to ensure the bed boundary layer separation (Sumer and Fredsøe, 2002). The rotation of the boundary layer over the surface of the structure leads to the formation of lee-wake vortex, as seen in Figure 2.3. Since there is a shear layer arising from the side edges of structure, the lee-wake vortices are generated (Sumer and Fredsøe, 2007).

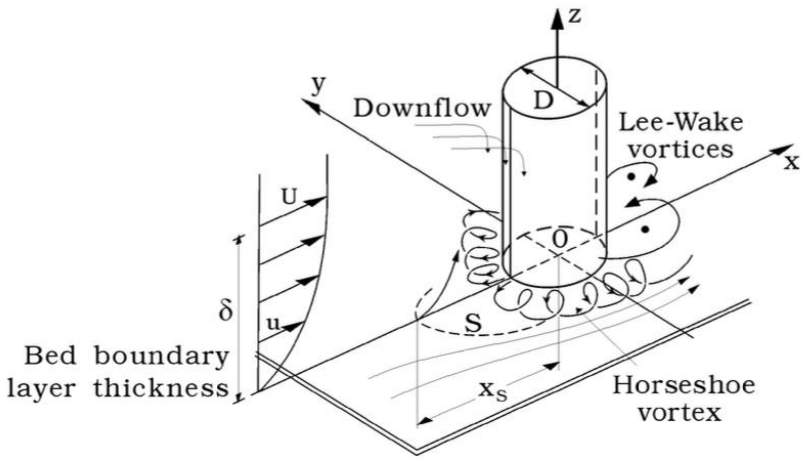

Figure 2.3 : Definition sketch. S: separation line (Sumer, 2007).

Umeda (2011) made an experimental study, which concerns about scour regime and scour morphology around a pile in waves for different pile diameters (D=22, 32, 48 and 76 mm). The mean grain size was $d_{50} = 0.28$ mm. The change in scour depth with KC number is given in Figure 2.4. According to the Figure 2.4, it can be indicated that the maximum scour depth can reach a value as high as 100% of the pile diameter. Zanke et al. (2011) presented a universal formula for the estimation of scour depth around a single cylinder under the combined waves and current. The results of their study were shown in a graph in Figure 2.5.

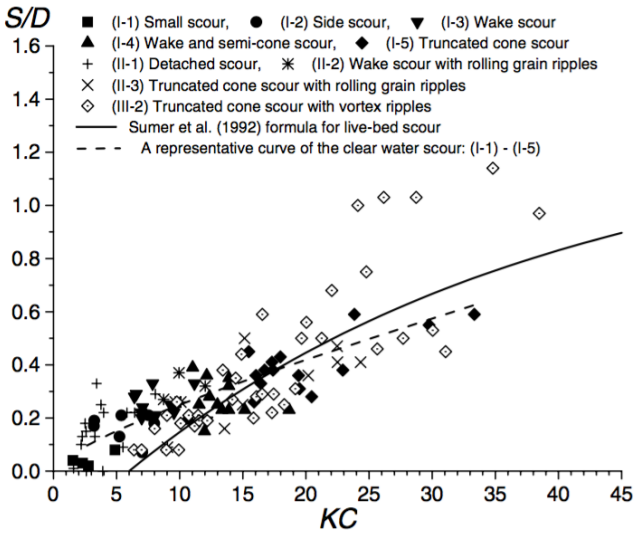

Figure 2.4 : Normalized equilibrium scour depth as a function of the KC number. The solid line indicates the empirical expression of Sumer et al. (1992) for the live-bed condition. The broken line is a representative curve of the present results for the clear-water condition (Umeda, 2011).

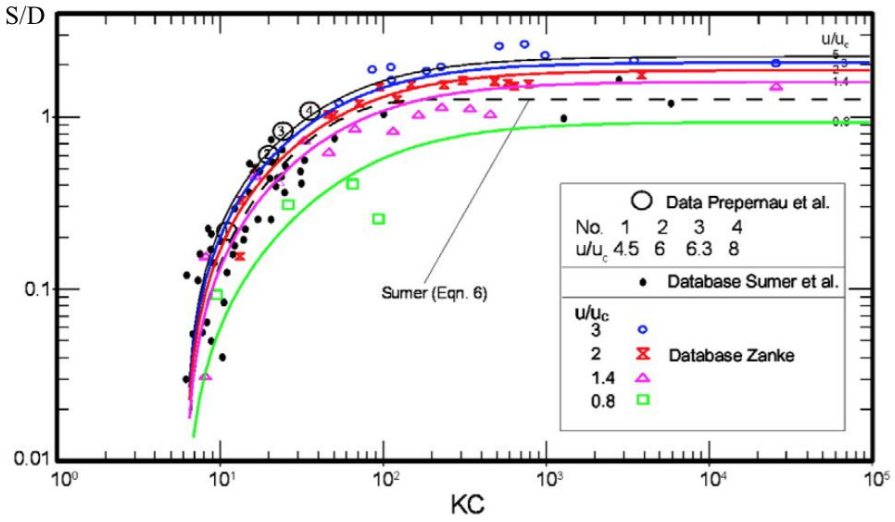

Figure 2.5 : Equilibrium relative scour depth S/D versus KC number for different u/u_c (Zanke et al., 2011).

2.4 Scour in Large Pile Regime

For engineers, scour around large marine structures is an important subject that must be investigated due to its wide application field, such as bridge piers, breakwater heads, wind turbine monopile foundations, platform legs, offshore gravity platforms, and so forth. If the structure size is so large, the flow is in the diffraction regime. Hence, in the large pile regime, the flow is unseperated on the contrary of slender pile regime, since the structure size is quite large when it is compared to the wavelength ($D/L > 0.1$). Therefore, horseshoe vortex and lee-wake vortex mechanisms cannot be observed in large pile regime (Sumer and Fredsøe, 2001). However, scour is generated in this regime, too. Hence, the scour in large pile regime must be explained by other mechanisms than vortex mechanisms. According to Sumer and Fredsøe (2001), the scour depends on mainly KC and D/L ratio. They found that the scour depth generally increases with these parameters. Khalfin (2007) showed the S/D dependence to KC number (Figure 2.7 and Figure 2.8).

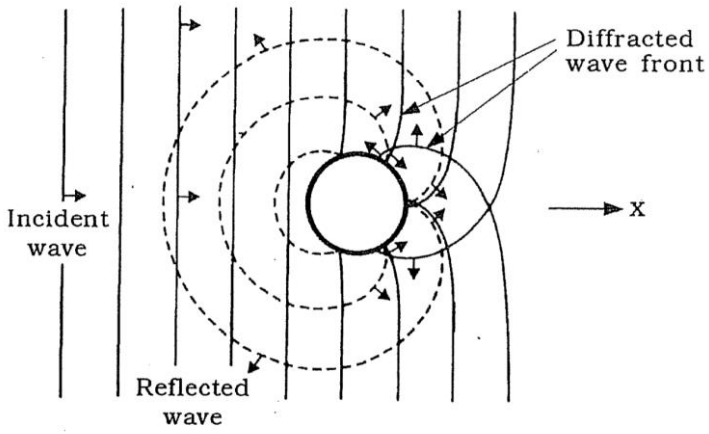

Figure 2.6 : Sketch of the incident, diffracted and reflected wave fronts around a pile (Sumer and Fredsøe, 2002, p. 288).

Khalfin (2007) have made an experimental study about scour around large diameter vertical cylinder under regular waves. He made two large series of experiments to study of local scour around a large diameter vertical cylinder exposed to waves, which was located on an erodible bed, composed of fine and coarse sand. Mean particle sizes were 0.25 mm for the first series of experiments, and 0.80 mm for the second series of experiments. The change in scour depth with KC number is given in the Figure 2.7. According to this study, maximum scour depth can reach the value of 7-8% of the pile diameter (Figure 2.7).

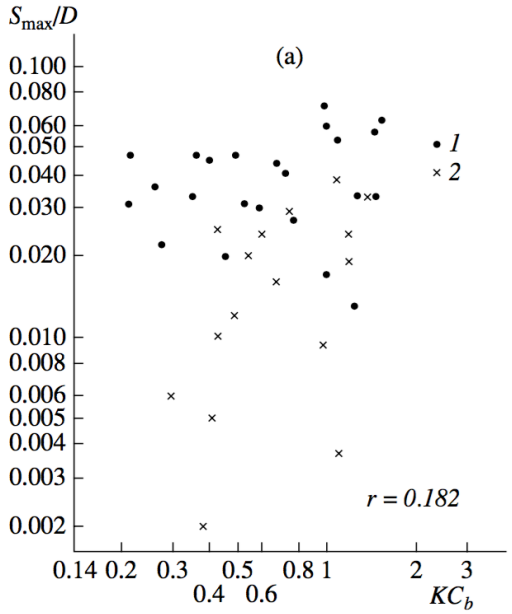

Figure 2.7 : Dependence of S/D on Keulegan-Carpenter number (1) $d_{50} = 0.25$ mm, (2) $d_{50} = 0.20$ mm, according to Sumer and Fredsøe (2001) (Khalfin, 2007).

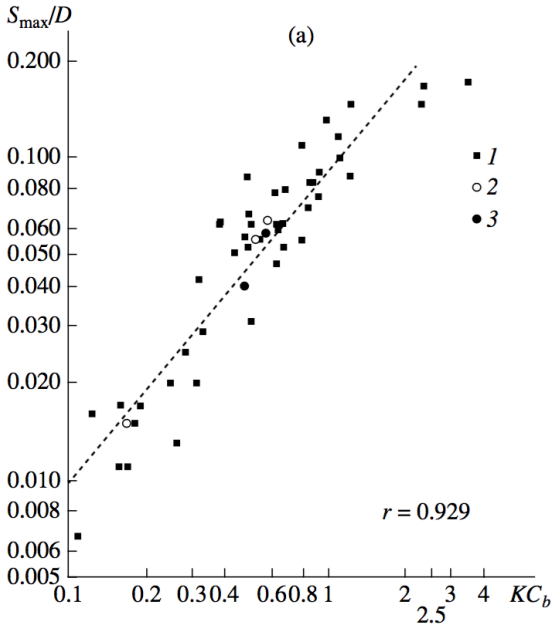

Figure 2.8 : Dependence of S/D on Keulegan-Carpenter number (1) $d_{50} = 0.8$ mm, (2) $d_{50} = 1.5$ mm (1) $d_{50} = 2.5$ mm (Khalfin, 2007).

Qi and Gao (2014) have studied experimentally on local scour around a large diameter monopile in combined waves and current. The scour depths, which they have observed for different wave heights were shown in Figure 2.9. The pile diameters were D=0.2 and D=0.08 m, the undisturbed near-bed current velocity was constant and it had a value of U_c=0.23 m/s. According to the Figure 2.9 (a), the scour depth can reach a value of 40% of the pile diameter.

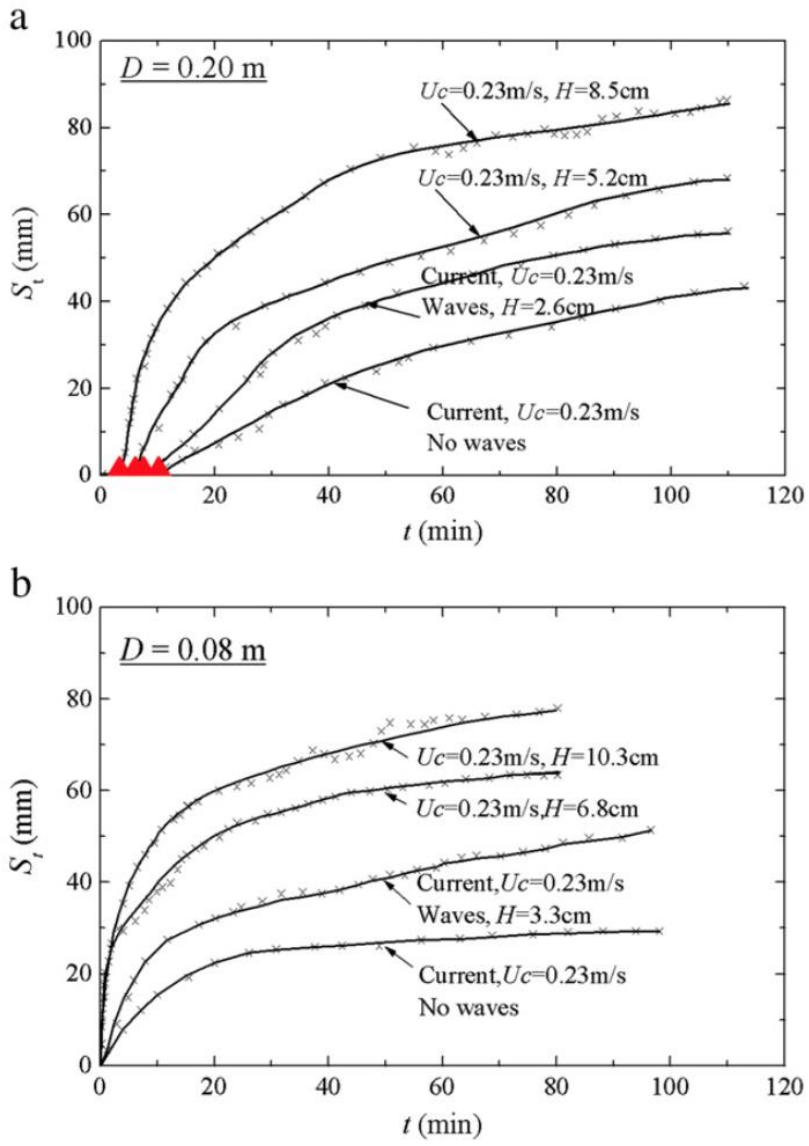

Figure 2.9 : Time development of scour depth measured at upstream edge of pile under waves with various wave heights following a current with a constant velocity U_c = 0.23 m/s (clear- water scour regime under current alone): (a) D = 0.20 m, (b) D = 0.08 m (Qi and Gao, 2014).

Rance (1980), Katsui and Toue (1988, 1993), Sumer and Fredsøe (2001) have studied experimentally about the scour around large vertical piles under wave effect. Sumer and Fredsøe (2001, 2002) have made some experiments to clarify the flow and scour process in the large pile regime. According to these researchers, it can be said that there are two types of flow in the case of large pile, namely, the phase resolved flow and the steady streaming around the structure, which are responsible for scour. In present study, diffraction regime and steady streaming will be explained in details.

2.4.1 Diffraction regime

In slender pile regime, the presence of the pile does not influence the flow, as mentioned in the preceding paragraphs. However, when the pile diameter to the wavelength (D/L) ratio gets larger, the structure presence will influence the incoming flow. Since the progressive waves impinge on the structure, reflected waves go through outwards, while there is diffracted waves formation on the sheltered side of the structure (Figure 2.6). This mechanism is called as diffraction (Sumer and Fredsøe, 2002). According to Isaacson (1979), the diffraction effect gains importance when D/L gets larger than 0.2. The relation between the Keulegan-Carpenter (KC_S) number, D/L ratio and diffraction effect is given in Figure 2.10. KC_S is defined by:

$$KC_S = \frac{2\pi a_S}{D} \tag{2.9}$$

Herein, a_S is the amplitude of the horizontal component of water-particle motion at the sea surface, according to the sinusoidal wave theory, calculated as follows:

$$a_S = \frac{H}{2\tanh(kh)} \tag{2.10}$$

In which, H is the wave height, h is the water depth and $k = \frac{2\pi}{L}$ is the wave number.

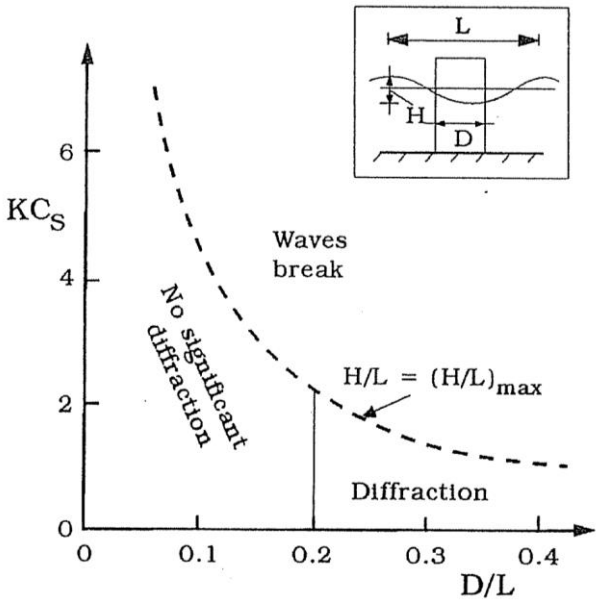

Figure 2.10 : Different flow regimes. Adapted from Isaacson (1979) (Sumer and Fredsøe, 2002, p. 290).

In Figure 2.10, the dashed line indicates the boundary of wave breaking. As shown in the Figure 2.10, the Keulegan-Carpenter numbers have pretty small values when the flow is in diffraction regime. Due to these small KC numbers, the flow around the pile is in unseperated flow regime. Since the main reason for horseshoe and lee-wake vortices formation is the flow separation, there will not be any vortex shedding and horseshoe vortex generation in diffraction regime (Sumer and Fredsøe, 2002). According to given information, D/L ratio is a parameter, which influences the flow and scour process in large pile regime.

2.4.2 Steady streaming

When a large vertical structure is placed in marine environment, it is subjected to progressive waves. The structure size is large when it is compared to the wavelength, so that there will be an interaction between the structure and the flow. As seen in Figure 2.6, the reflected waves moves outward from the cylinder and the diffracted waves are generated on the sheltered side of the structure. Steady streaming around the cylinder is a kind of flow induced by these wave fields (Sumer and Fredsøe, 2002). Sumer and Fredsøe (1997, 2001) have studied in order to explain the steady streaming mechanism. The experimental results of their study indicated that, steady streaming is caused by the presence of pile itself, it does not depend on other effects. When a circular cylinder is exposed to oscillatory flow, there will be an interaction between the flow and the cylinder, which will cause a non-zero period averaged flow field around the cylinder. This mechanism is called as steady streaming (An, Chang and Zhao, 2009).

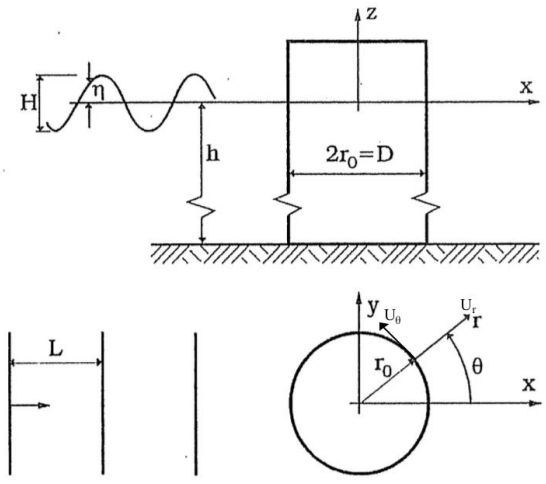

Figure 2.11 : Definition sketch (Sumer and Fredsøe, 2002, p. 289).

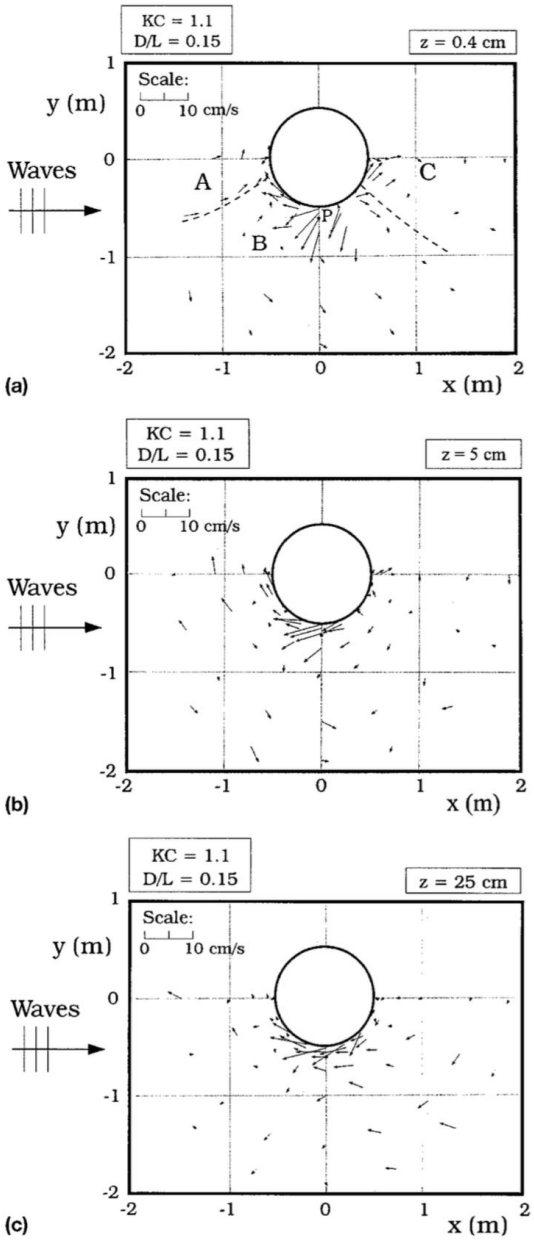

Figure 2.12 : Vector diagram of period averaged velocities (steady streaming) at distance from bed of (a) $z = 0.4\ cm$; (b) $z = 5\ cm$; (c) $z = 25\ cm$ (Sumer and Fredsøe, 2001).

Sumer and Fredsøe (2001) made velocity measurements at three different distances from the bed, where z =0.4, 5 and 25 cm, to express steady streaming around the cylinder. Period averaged velocities are defined by:

$$U_r = \frac{1}{T}\int_0^T \overline{u_r}\, dt$$

$$U_\theta = \frac{1}{T}\int_0^T \overline{u_\theta}\, dt \qquad (2.11)$$

In equation 2.11, T is the wave period, U_r and U_θ are plan view components of steady-streaming velocity. The direction of U_r and U_θ can be seen in Figure 2.11.

When the velocity measurements in undisturbed case are compared with the velocities measured near the pile at the same depth, it can be deduced that the velocities are quite smaller in undisturbed case flow. Therefore, the period averaged flow is essentially due to the presence of pile (Sumer and Fredsøe, 2001). In Figure 2.12, the wave induced steady streaming around the structure can be seen clearly. Acoording to the experimental results, it can be said that, the velocity of streaming can have values of 25% of the maximum value of the undisturbed wave velocity at the bed. Another important observation, which is made in their experiments, is about the regions A, B and C given in the Figure 2.12 (a). In A region, the streaming is towards the pile, contrary to the streaming direction of B and C region. The observed large radial velocities in the region B are due to the bed boundary layer responding to the reflected waves. Because there was no such velocities measured in the pile absence (Sumer and Fredsøe, 2001). This result proves that, steady streaming around the structure is caused by the presence of the large structure.

Schlichting (1979, p. 428) indicates that two-dimensional steady streaming around the cylinder is formed when the cylinder is under the effect of oscillatory flow (Figure 2.13).

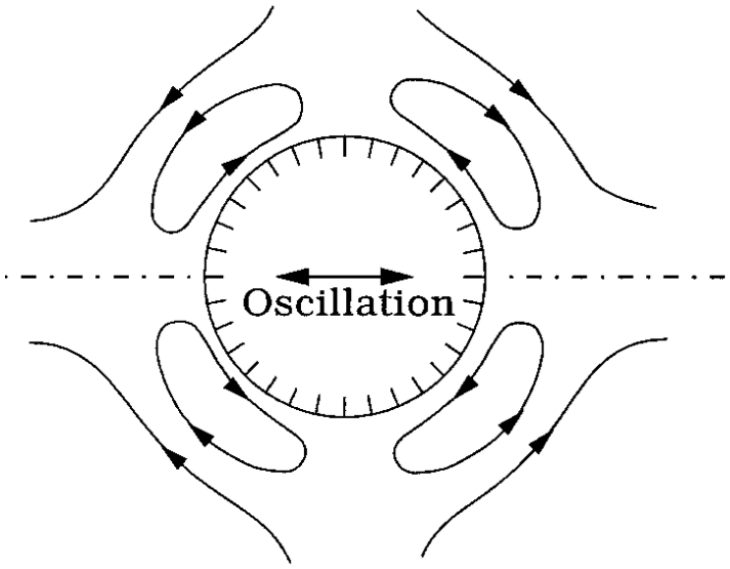

Figure 2.13 : Steady streaming around a cylinder subject to a plane oscillatory flow. 2-D case (Sumer and Fredsøe, 2002, p. 301).

An, Cheng and Zhao (2009) have investigated the oscillatory flow induced steady streaming around a circular cylinder by using a numerical method for different KC numbers, which has the values between 2 and 40 (Figure 2.14). In Figure 2.14 (a), it can be seen that the steady streaming is symmetric both x and y-axis. This rstreaming structure is similar with the results of an experimental study, which was conducted by Van Dyke (1982). However, it must be noted that these results were observed under low KC and Re numbers.

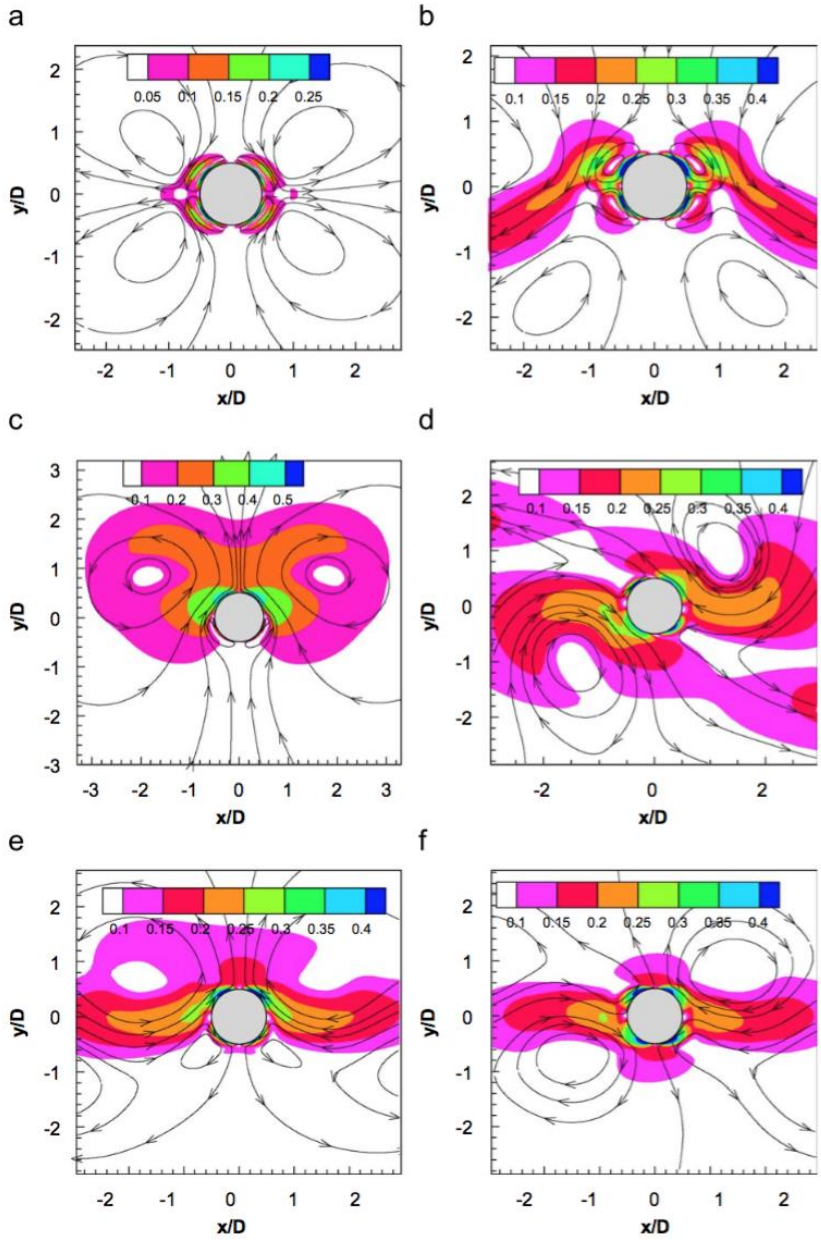

Figure 2.14 : Streamlines of steady streaming velocity and magnitude contours of steady streaming velocity (U_s/U_m) in six vortex shedding regimes (a) KC=3.5, (b) KC=5, (c) KC=10, (d) KC=16, (e) KC=26, (f) KC=33 (An, Cheng and Zhao, 2009).

2.4.3 Streaming induced scour mechanism

The steady streaming mentioned in the preceding paragraphs disturbes the bed and creates a different flow mechanism near the pile. Hence, if the bed is erodible, the steady streaming leads to the formation of a scour. Sumer and Fredsøe (2001) gave the final bed topography around the cylinder after one of the experiments they conducted after the equilibrium stage is reached, namely after 8 hours test time (Figure 2.10).

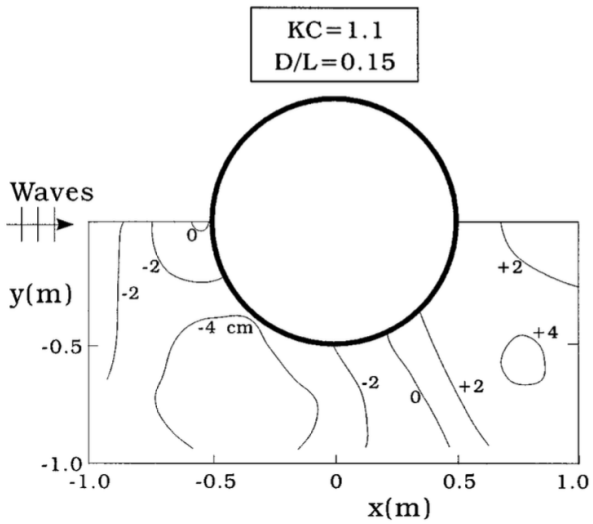

Figure 2.15 : Contour plot of bed topography in equilibrium stage; live bed ($\theta > \theta_{cr}$); numerical figures indicate scour ($-$) and deposition ($+$) in centimeters (Sumer and Fredsøe, 2001).

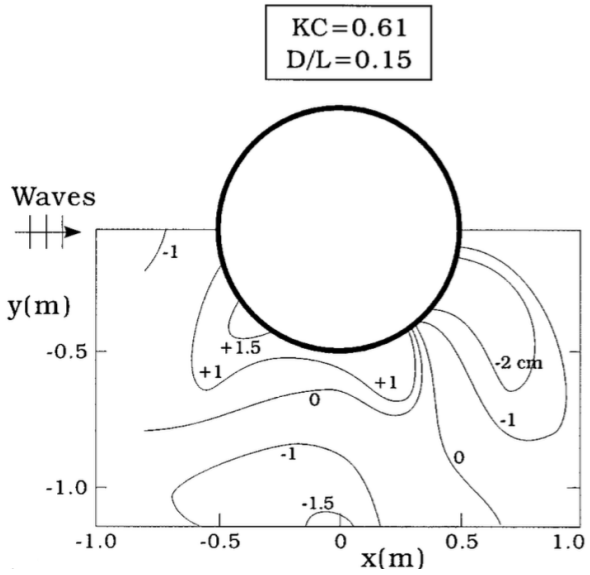

Figure 2.16 : Contour plot of bed topography in equilibrium stage; live bed ($\theta > \theta_{cr}$); numerical figures indicate scour ($-$) and deposition ($+$) in centimeters (Sumer and Fredsøe, 2001).

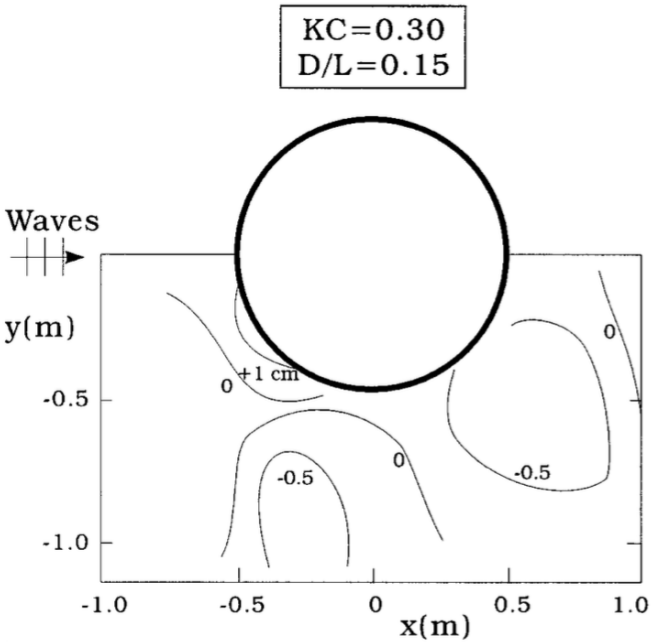

Figure 2.17 : Contour plot of bed topography in equilibrium stage; live bed ($\theta > \theta_{cr}$); numerical figures indicate scour $(-)$ and deposition $(+)$ in centimeters (Sumer and Fredsøe, 2001).

When the Figure 2.12 and Figure 2.15 are compared, it can be noted that, in the erodible bottom case, the sediment stirred up and brought up into suspension under the wave effect is moved away from the B region. This mechanism causes a scour hole formation near the cylinder. Since the streaming direction is from B to C region, there is a deposition observed in C region. As can be seen from Figure 2.15, scour depth can have a value, which equals to 4% of cylinder diameter (Sumer and Fredsøe, 2001).

3. EXPERIMENTAL SETUP

3.1 Experimental Facilities

The experiments were conducted in a regular wave flume, which is located in İstanbul Technical University Hydraulics Laboratory. The flume is 22.5 m in length, 1 m in width and 0.5 m in height (Figure 3.1). The walls of flume were made of glass. The flume base was made of concrete and it was smooth. In order to fill the wave flume, the water comes from the water tower with gravity flow by pipes, was used. This water accumulated in the stilling basin of the flume before it rises and fills the flume. In order to generate regular waves, a palette of flap type was used (Figure 3.1). In order to perform the experiments, two twin cylinders were used. These cylinders, which were made of PVC, had the same diameter of $D = 22.5$ cm and have the same length of 50 cm. The cylinders were placed vertical and they were flush mounted to both the flume base and wall of the flume. Water seepage was prevented among the cylinders and the flume base, also between the cylinders and the flume wall. The experiments were performed for different space ratios x/D between the cylinders. Here, x indicates the distance between the centers of cylinders (Figure 3.2). In this study, rigid bed experiments and actual scour bed experiments were conducted. The first experiments of rigid bed and actual scour bed was conducted with single cylinder (with the experimental cylinder), which the pressure measurement was made. Rest of the experiments was handled by using the experimental and dummy cylinders. In the rigid bed experiments, the bed surface of the flume was smooth. For the following experiments, a sand pit, which is 3 m in length and 1 m in width and 6 cm in height, was placed on the flume base. In order to provide the wave generation as it supposed to be, the sand pit was located at a distance of 7 m from the wavemaker.

There were two kinds of measurements made in the experiments, which are pressure measurements on the surface of experimental cylinder above 5 cm from the bed and velocity measurements at undisturbed bed (at 3 m distance from the sand pit). And on the scour bed experiments, the bottom was scanned before and after the tests.

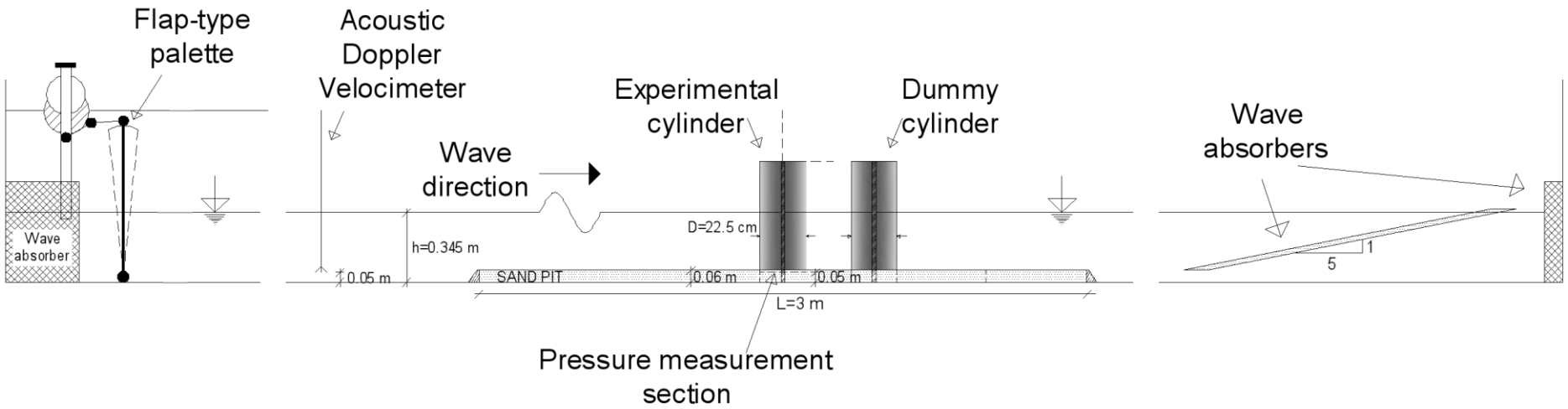

Figure 3.1 : Profile view of the wave flume-scour bed experiments.

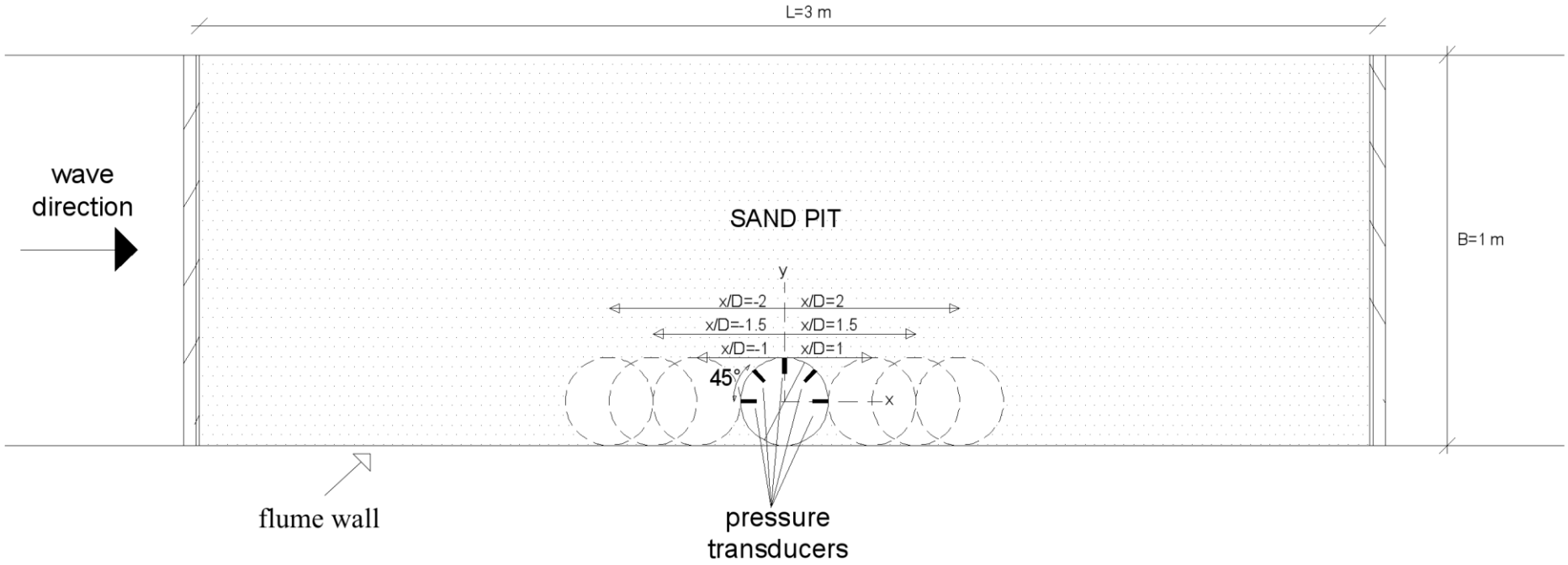

Figure 3.2 : Plan view of the wave flume-scour bed experiments for different x/D ratios.

3.2 Sieve Analysis

In the experiments, quartz sand was used as bed material. This sand was sieved and the finer percent by weight passing through the sieves which have 1.19 mm, 1 mm, 0.84 mm, 0.71 mm, 0.50 mm, 0.25 mm sieve openings respectively was found, and grain size distribution was plotted (Figure 3.3).

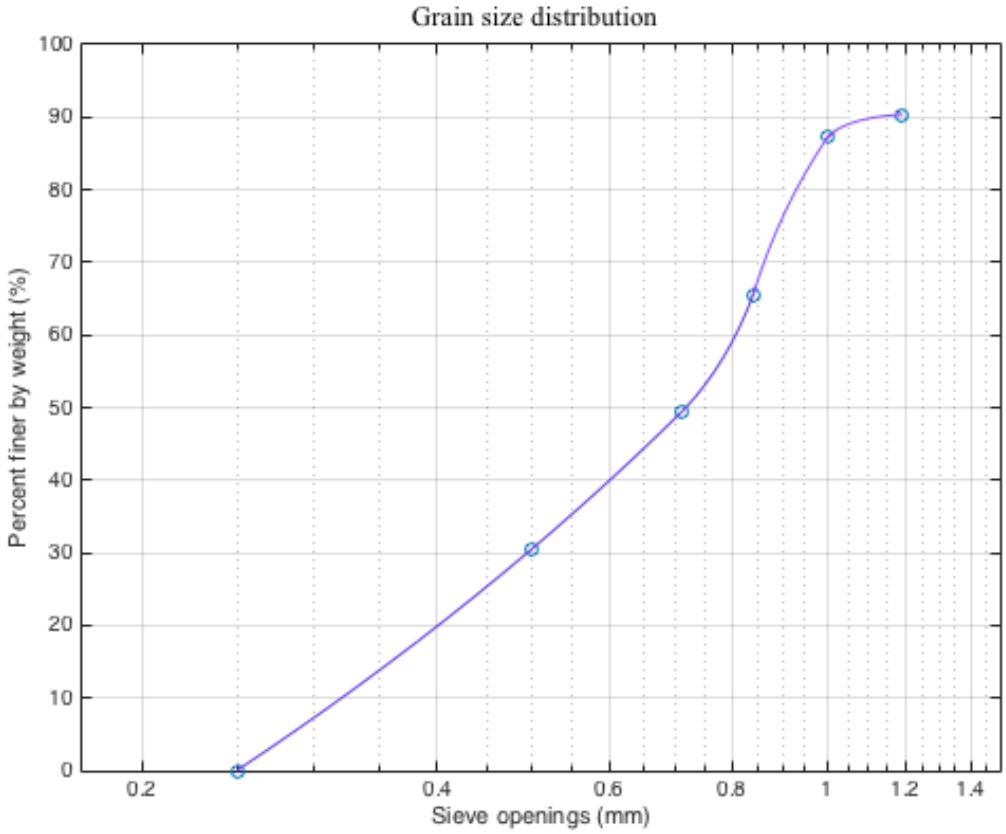

Figure 3.3 : Sediment gradation.

According to the sieve analysis result, the mean grain size d_{50} is obtained as 0.72 mm. The geometric standard deviation, σ_g, is defined as:

$$\sigma_g = \sqrt{\frac{d_{84}}{d_{16}}} \tag{3.1}$$

In equation 3.1, σ_g, is the geometric standard deviation. From the Figure 3.3, it can be seen that $d_{84} = 0.97$ mm and $d_{16} = 0.38$ mm. Hence, the geometric standard deviation is calculated as 1.6.

3.3 Measuring Instruments

3.3.1 Pressure transducers and data acquisition system

In the experiments, five Mesens $MPS500.010$ series pressure transducers (Figure 3.4) with $\pm 0.5\%$ FS accuracy at 10 V DC were used in order to determine the pressure heights on the surface of experimental cylinder. Four of the pressure transducers were with a range of $0 - 100$ mbar and one of the transducers was with a range of $0 - 250$ mbar. The transducers were flush mounted on the surface of the experimental cylinder 5 cm above from the flume surface at 45° intervals (Figure 3.2). These pressure transducers were connected to a data acquisition system named Testbox 2010 (Figure 3.5). This device is an amplifier, which has signal amplifiers at channel inputs. It digitizes the analog pressure data. Power input is 12 V DC. The imported data was stored in computer by using the computer program, Testlab Dynamic.

Figure 3.4 : Mesens $MPS500.010$ series pressure transducers, dimensions in mm.

Figure 3.5 : Pressure data acquisition system (Testbox 2010).

3.3.2 Vectrino I

Vectrino is an acoustic velocimeter, which was developed by NORTEK. This device measures velocity by using the logic of Doppler shifting processing. It sends an acoustic signal to the water; in return it receives an audio echo and it measures the difference at the elevation and frequency. At the end of this process, it acquires the velocity data from the phase shift. The vectrino has a sampling rate of 200 Hz with the Vectrino Plus Program and it has 4 receivers. One of these receivers is in x direction, one of them is in y direction and two of them are in direction z. The angle between the receivers and the main probe is 30°. With the data received from these 4 receivers, a three-dimensional velocity data is obtained (Vectrino User Guide, 2004). In the experiments, in order to define the velocities in undisturbed bed, the vectrino is placed 5 cm above the undisturbed bed (at the same height with the pressure transducers).

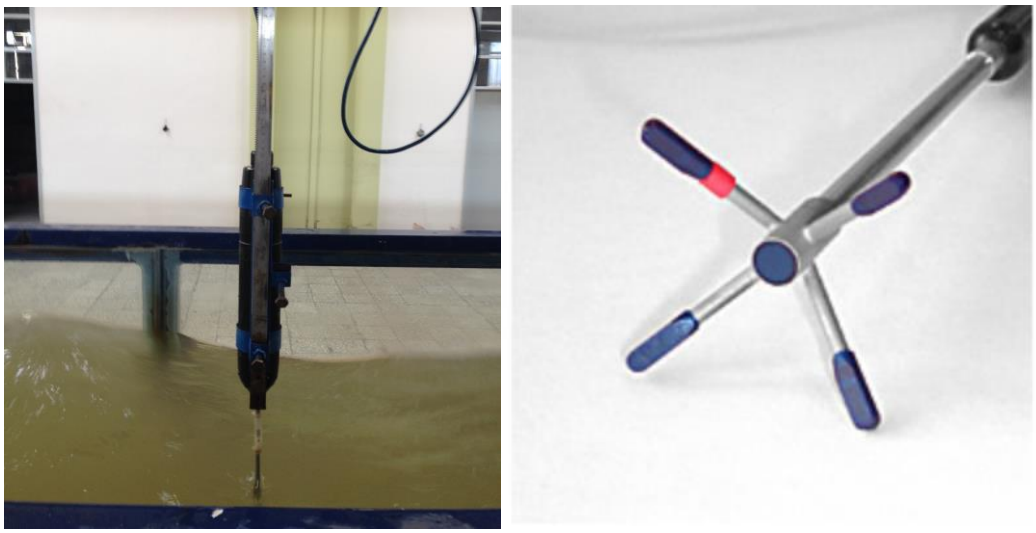

Figure 3.6 : Acoustic Doppler Velocimeter (ADV), which was used in the experiments (Vectrino I).

3.3.3 Laser scanner

In the experiments, Leica Scanstation C10 model laser scanner was used in order to determine final topography of the erodible bottom and compare it with the initial condition. Leica Scanstation laser scanner is compact, pulsed and very high-speed laser scanner (Figure 3.7). By using this device, a three dimensional model can be generated on a computer after gathering high-definition data in couple of minutes and analyzed by using several computer software developed for engineers. This model can scan 360° in vertical direction and 270° in horizontal direction. The maximum measurement distance for the scanner is 300 m, while the minimum distance is 0.1 m. The scan rate is 50000 point/sec. Power supply is 15 V DC.

At the beginning and at the end of each experiment, the sand pit was scanned and with the data received, the elevation differences between the initial and final bottom conditions are obtained by using laser scanner.

Figure 3.7 : Leica laser scanner.

3.4 Test Conditions

In this thesis, an experimental study was made that deals with the scour around a pile supported wharf and the forces acting on the pile surface. Two types of experiments, which are rigid bed experiments and actual scour bed experiments, were held in order to clarify the flow mechanism around the cylindrical vertical large piles, to obtain the scour around the structure and to determine the forces acting on the surface of the pile. In all the tests, the cylinders were flush mounted to the flume base and flume wall (Figure 3.2). Two types of cylinders were used, namely measurement cylinder and dummy cylinder. Pressure measurement was made on the surface of the measurement cylinder, where any measurements were made on dummy cylinder. First of all, rigid bed experiment for the single cylinder (measurement cylinder) case was made. Secondly, the experiments on rigid bed for different gap ratios between the measurement and dummy cylinders, namely $x/D = 1$, $x/D = 1.5$, $x/D = 2$, was conducted. For actual erodible bed experiments, a rectangular shaped sand pit, which was 3 m in length, 1 m in width and 6 cm in depth, was placed at a distance of 7 m from the wavemaker and the experiments were repeated for single cylinder and tandem cylinder cases on live bed scour. In all the tests, regular waves, which have the same wave conditions, namely the same wavelength (L), wave height (H) and wave period (T), were generated. The wave height is 0.13 m and the wave period is 0.88 s. The water depth is 34.5 cm According to the sinusoidal wave theory; the wavelength is calculated as follows:

$$L = L_0 \tanh(kh) \tag{3.2}$$

Herein, L_0 is the deep-water wavelength (Equation 3.3) and k is the wavenumber (Equation 3.2) and h is the water depth above the sediment and it equals to 28.5 cm. Where g is the acceleration of gravity, the deep-water wavelength given as follows:

$$L_0 = \frac{gT^2}{2\pi} \tag{3.3}$$

$$k = \frac{2\pi}{L} \tag{3.4}$$

From the given equations, L_0 is calculated as 1.26 m and $tanh\ (kh)$ is taken from the sinusoidal wave tables as 0.926. According to these values, the wavelength is calculated as 1.15 m. Hence, D/L is found as 0.19.

Since the wave conditions were the same in all the tests, KC number had the same value as well. KC number is defined as given by (Sumer and Fredsøe, 2002):

$$KC = \frac{U_m T}{D} \tag{3.5}$$

In which, U_m is the maximum value of the orbital wave velocity of water particles at the bed, given as:

$$U_m = \frac{\pi H cosh(k(z+h))}{T sinh(kh)} \tag{3.6}$$

In equation 3.6, z is the vertical distance measured from the mean water level, which is equal to $-h$ at the bed. From the equation 3.5 and 3.6, KC and U_m can be found as 0.74 and 0.18 m/s, respectively. The maximum value of bed shear velocity in waves, namely U_{fm} was calculated by using equation 3.10 and it was found as 0.03 m/s. As mentioned in the preceding paragraphs, velocity measurements were made by ADV and the measurement results were compared with the calculations. The velocity measurement results can be seen in Figure 3.8.

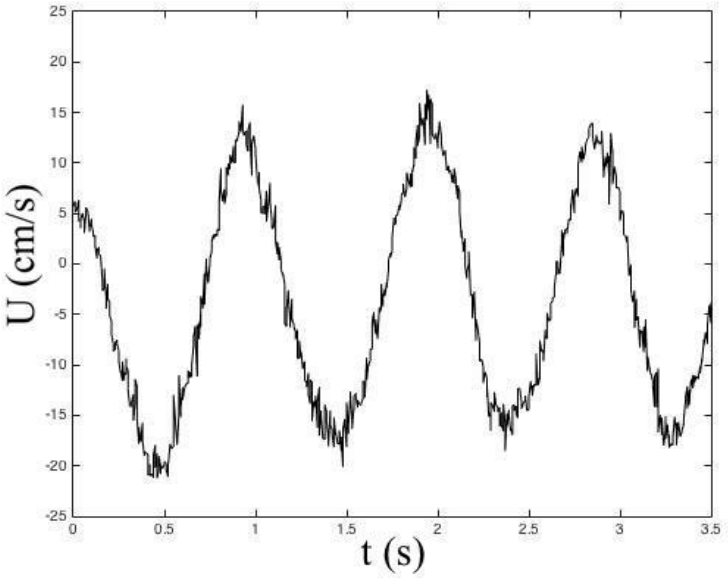

Figure 3.8 : Horizontal values of the orbital wave velocity above 5 cm from the flume bottom, at the undisturbed bed.

According to the Figure 3.8, U_m (the maximum value of the horizontal orbital wave velocity) can be determined as $0.17 \sim 0.18$ m/s. Therefore, it can be said that the measurements and the calculations are consistent with each other.

As written in the preceding paragraphs, the scour experiments were made on live bed. Where a is the amplitude of near-bed wave orbital motion (Equation 3.7), k_N is the equivalent sand roughness of the bed and it is equal to 0.18 cm (Equation 3.8). When the equation 3.9 was prevailed, the wall category is transitional (Sumer, 2013). Since $\frac{k_N U_{fm}}{\nu}$ is calculated as 54 by using the equation 3.9, transitional category wall is valid. The wave friction factor f_w is calculated as 0.05 by using equation 3.10. (Equation 3.10 was suggested by Kamphuis (1975)), s is the dimensionless specific weight of the sediment and it has a value of 2.65, Shields parameter, θ can be calculated as 0.078 by following the equations (Fredsøe and Deigaard, 1992) given as follows:

$$a = \frac{H cosh(k(z+h))}{2 sinh(kh)} \tag{3.7}$$

$$k_N = 2.5 d_{50} \tag{3.8}$$

$$5 < k_N \frac{U_{fm}}{\nu} < 70 \tag{3.9}$$

$$f_w = 0.4 (\frac{a}{k_N})^{-0.75}, \qquad \frac{a}{k_N} < 50 \tag{3.10}$$

$$U_{fm} = U_m \sqrt{\frac{f_w}{2}} \tag{3.11}$$

$$\theta = \frac{U_{fm}^2}{g d_{50}(s-1)} \tag{3.12}$$

The critical Shields parameter, which is given by Sumer and Fredsøe (2002) as 0.05, therefore it can be said that live bed scour was prevailed.

The wave energy is given as follows (Holthuijsen, 2010):

$$\mathrm{E} = \frac{1}{8}\gamma H^2 \tag{3.13}$$

The wave power P is assumed to be constant and it is defined as:

$$\mathrm{P} = \frac{1}{8}\gamma H^2 c_g B \tag{3.14}$$

In equation 3.13, H is the wave height B is width and c_g is the group velocity. These parameters changes in the vicinity of the structure, since the flume width becomes narrow due to the presence of structure and this will affect the wave height. Where B_0 is the flume width and B_1 is the narrowed flume width, the relationship between these parameters and Shields parameter can be written as follows (Equation 3.15 was written by using the equation 3.14, equation 3.6 and equation 3.12):

$$\frac{B_1}{B_0} = \frac{H_0^2}{H_1^2} \cong \frac{U_{m_0}^2}{U_{m_1}^2} \cong \frac{\theta_0}{\theta_1} \tag{3.15}$$

In equation 3.13, Shields parameter in the vicinity of the structure was shown as θ_1 and Shields parameter in the indisturbed bed was shown as θ_0. The relationship between these parameters can be given by equation 3.16. In can be indicated that, Shields parameter in the vicinity of the structure is 1.3 times larger than the Shields parameter at the undisturbed bed in this case, this effect will increase the sediment mobility in the vicinity of the structure and it will cause a scour formation around the structure.

$$\theta_1 \cong 1.3\theta_0 \tag{3.16}$$

4. EXPERIMENTAL RESULTS AND DISCUSSION

4.1 Scour Mechanism

4.1.1 Vortex induced scour

As detailed in the preceding paragraphs, the structure, which built in the marine environment, disturbs the flow in its neighbourhood and eventually there is a scour generation around the structure. In slender pile regimes, horseshoe and lee wake vortices are mainly responsible of scour because of the flow seperation. Although there is no flow separation around the large piles ($D/L > 0.1$) and no horseshoe or lee-wake vortices formation, there was vortex generation on the upstream side of the cylinder in this experimental study (Figure 4.1). It may be said that, this vortex mechanism is similar to horseshoe vortex. The period of this vortex was recorded as 0.8 s. It was visualized and given in Figure 4.2.

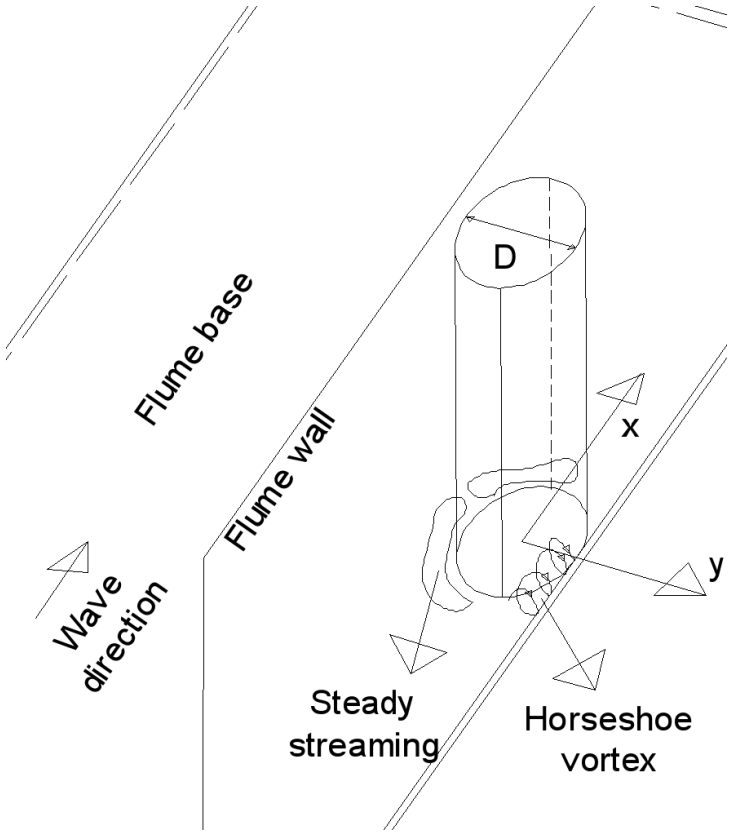

Figure 4.1 : Definition sketch of horseshoe vortex generation.

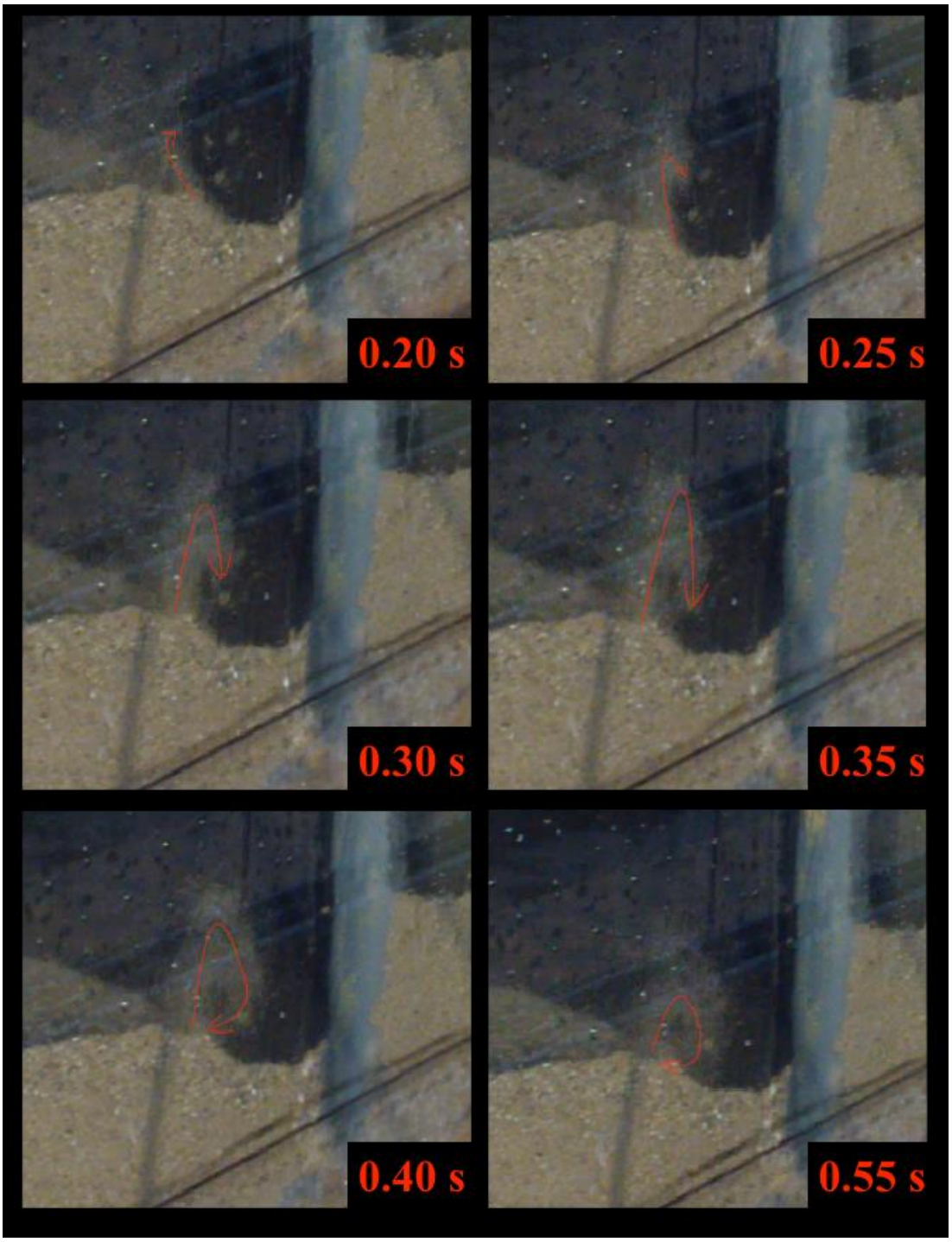

Figure 4.2 : Visualization of vortex generation in front of the measurement cylinder for single cylinder case, vortex period is 0.8 s.

In all the tests, vortex formation was observed in the wave coming side, between the flume wall and the cylinder. This vortex was caused by the presence of the flume wall. The wall presence created a negative pressure gradient and it caused a separation on the wave boundary layer on the upstream side of the cylinder. Therefore, the separated boundary layer turned into a spiral vortex between the

structure and flume wall (Figure 4.1 and Figure 4.2). And this vortex mechanism caused scour generation in this region (Figure 4.3).

Figure 4.3 : The vortex induced scour between the flume wall and the cylinder at the incoming wave side, $x/D = 2$ (measurement cylinder is at the incoming wave side).

4.1.2 Streaming induced scour

According to Sumer and Freds ø oe (2002), the wave induced phase-resolved velocities around the cylinder can be 2 times larger than the maximum undisturbed wave velocity. Therefore, the Shields parameter in the vicinity of the structure can be larger than the Shields parameter at the undisturbed bed. In erodible bed condition, wave induced steady streaming transports this sediment. In all the experiments, scour and deposition process around the structure was observed during the tests by a camera system. After the tests, final bed topographies were scanned and it was visualized, which the scour and deposition regions were showed in details (Figure 4.4, Figure 4.6, Figure 4.9, Figure 4.11, Figure 4.13, Figure 4.16, Figure 4.19). Additionally, contour lines for the final bed topography were drawn and shown in Figure 4.5, Figure 4.8, Figure 4.10, Figure 4.12, Figure 4.15, Figure 4.18, Figure 4.19. The datum plane was taken as the average value of the maximum and the minimum bottom level and the scour and deposition depth were showed in cm in figures (Figure 4.4, Figure 4.5, Figure 4.6, Figure 4.8, Figure 4.9, Figure 4.10, Figure 4.11, Figure 4.12, Figure 4.13, Figure 4.15, Figure 4.16, Figure 4.18, Figure 4.19, Figure 4.20). The streaming zones were demonstrated as sketches for all the tests. The streaming cells formed around the cylinder were presented in figures (Figure 4.5, Figure 4.7, Figure 4.10, Figure 4.12, Figure 4.14, Figure 4.17, Figure 4.21). These streaming zones were drawn by using the maps of scour and deposition pattern, which were obtained and visualized by scanned data (Figure 4.4, Figure 4.6, Figure 4.9, Figure 4.11, Figure 4.13, Figure 4.16, Figure 4.19).

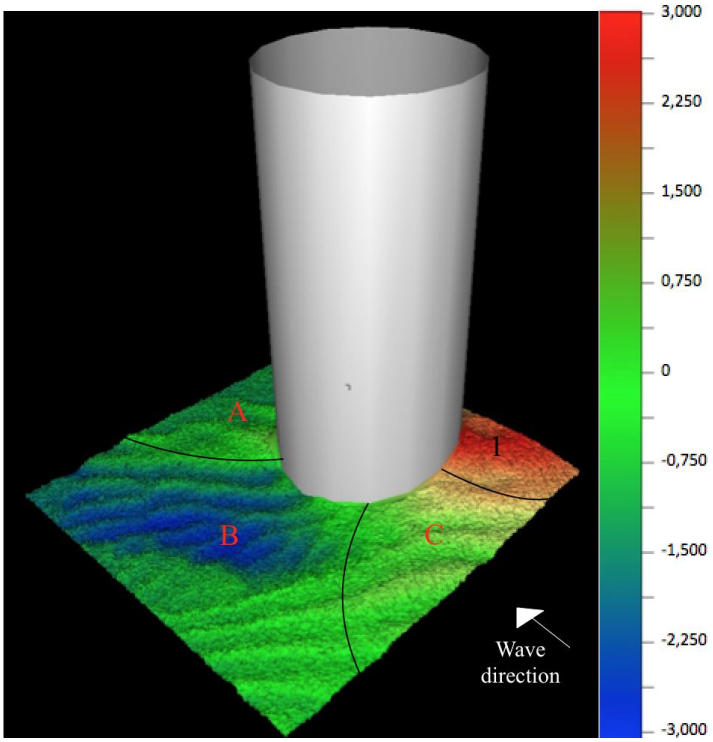

(a)

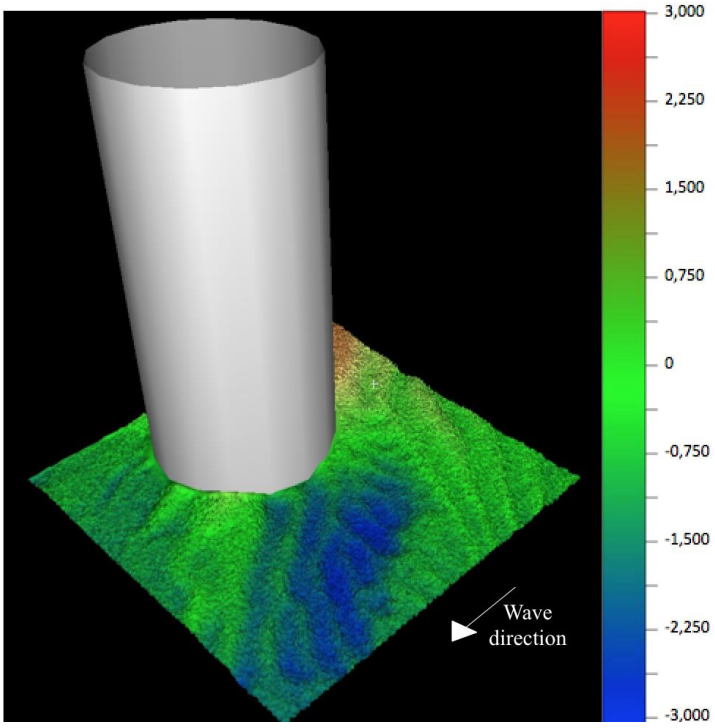

(b)

Figure 4.4 : The scour and deposition pattern around the cylinder for single cylinder, live bed, a) incoming wave side, b) sheltered side (The legend values are in cm).

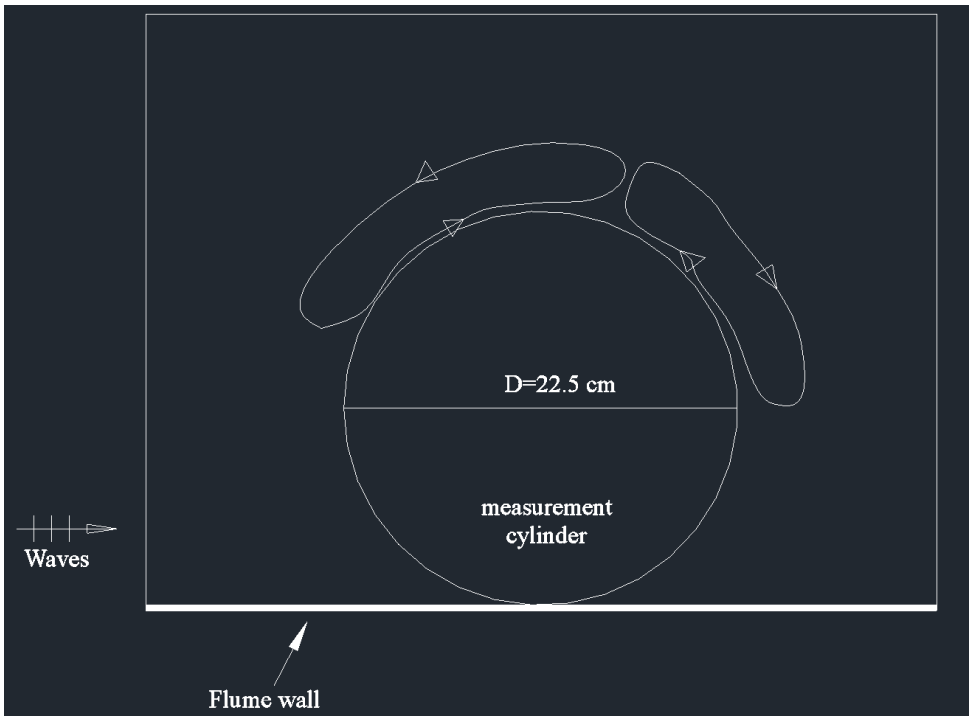

(a)

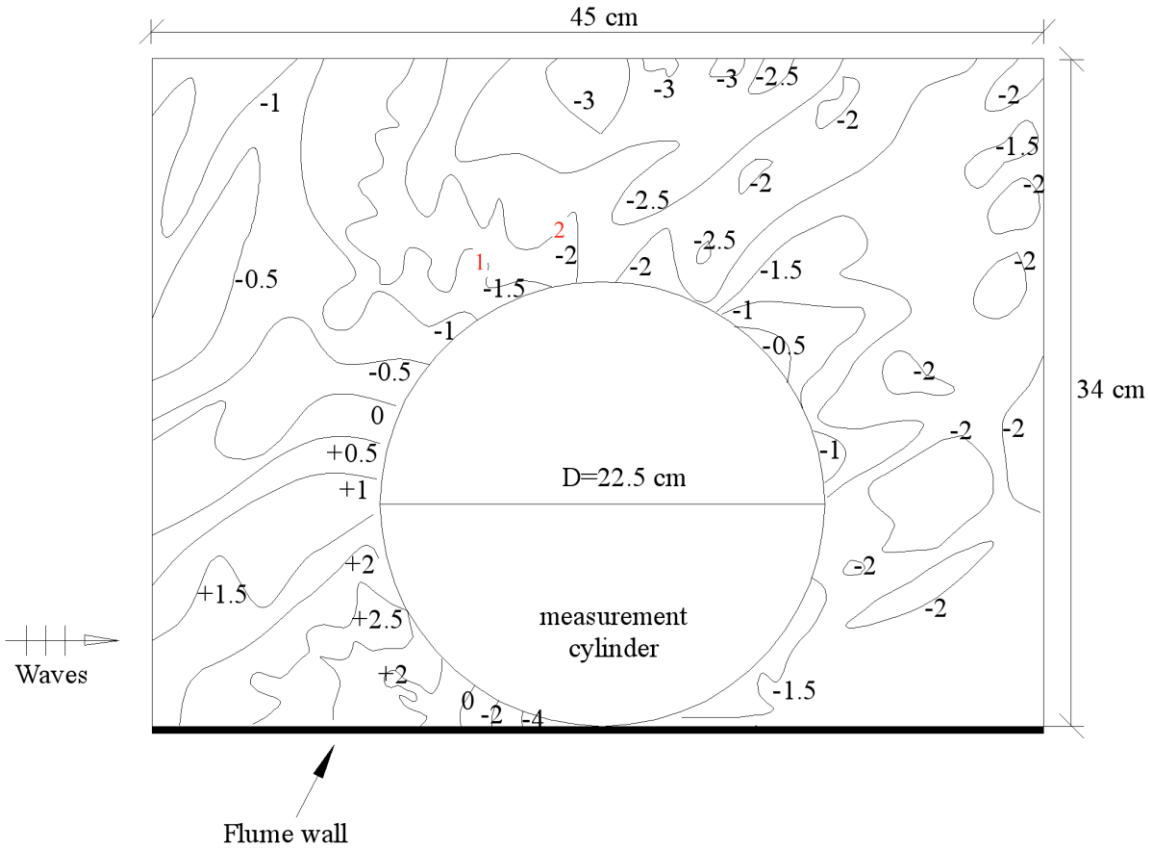

(b)

Figure 4.5 : For single cylinder case and live bed, a) definition sketch of streaming around the cylinder, b) contour lines for the final bed topography (Scour and depositions are in cm).

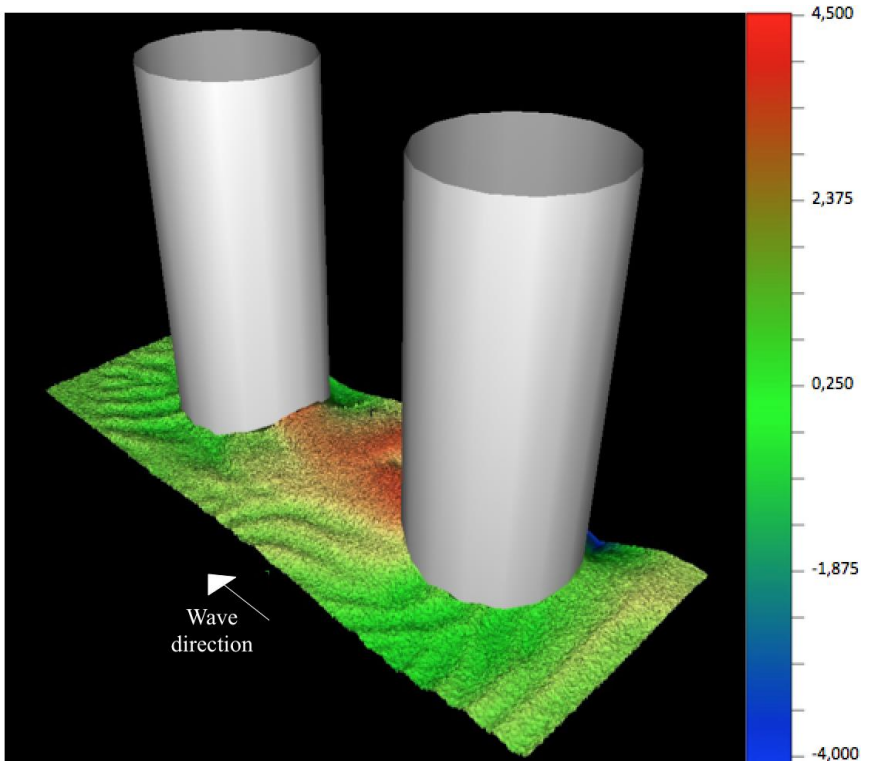

(a)

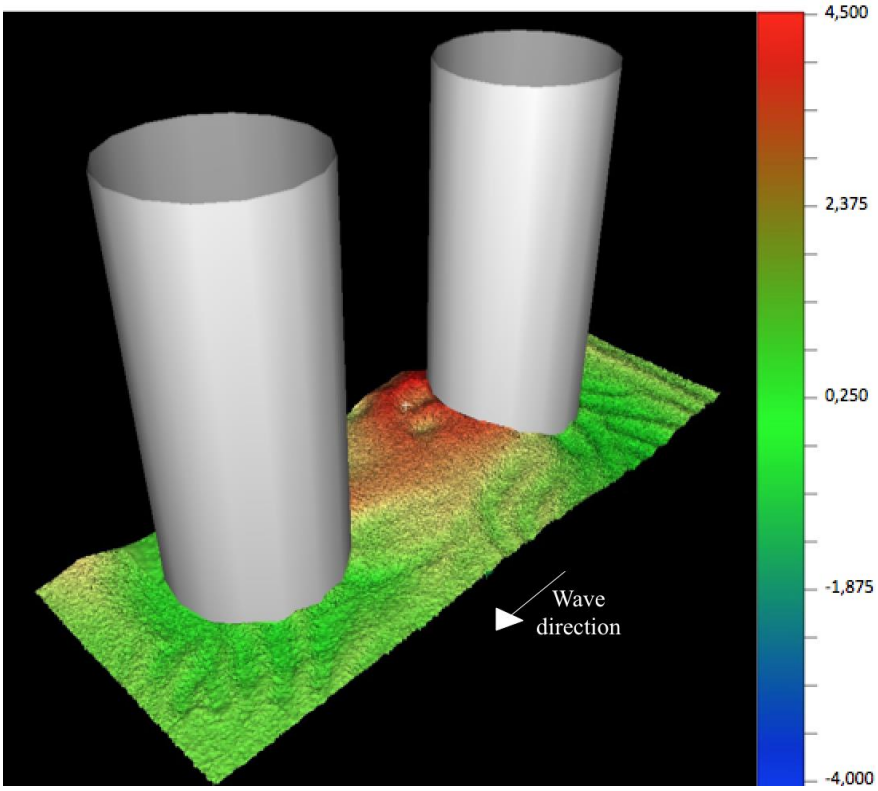

(b)

Figure 4.6 : The scour and deposition pattern around the cylinder for $x/D = 2$ (measurement cylinder is at the incoming wave side), live bed, a) incoming wave side, b) sheltered side (The legend values are in cm).

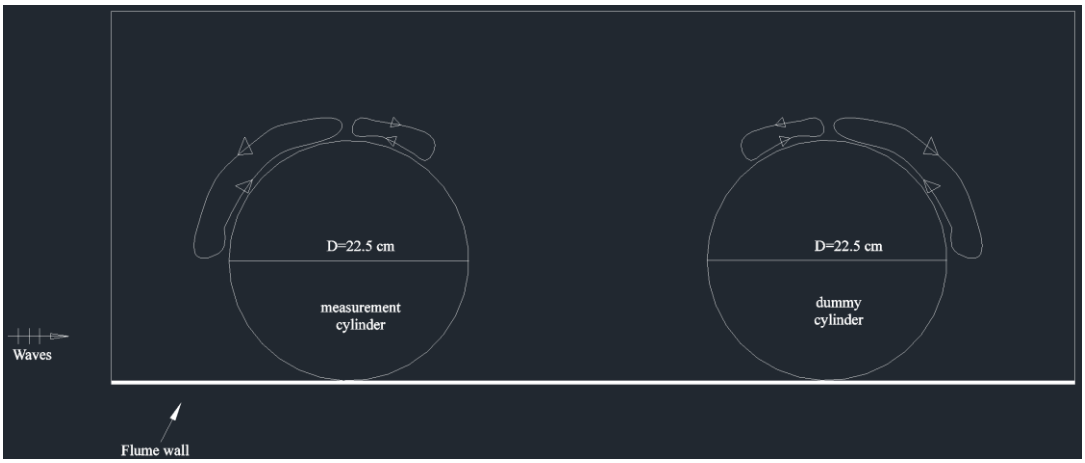

Figure 4.7 : For $x/D = 2$ (measurement cylinder is at the incoming wave side) and live bed, definition sketch of streaming around the cylinder.

Streaming cells, which were shown in Figure 4.5 (a), Figure 4.7 and Figure 4.10 (a), Figure 4.12 (a), Figure 4.14, Figure 4.17 and Figure 4.21 were drawn by the help of Schlichting's study (1979). The final bed topography visualizations shown in Figure 4.4, Figure 4.6, Figure 4.9, Figure 4.11, Figure 4.13, Figure 4.16, Figure 4.19 helped to sketch these cells for each of the experiments. From the Figure 4.5 (a), Figure 4.7, Figure 4.10 (a), it may be said that the streaming cells are symmetric due to the centreline of the system. According to the sketched streaming cells, it may be indicated that the streaming zones are similar for the single cylinder and $x/D = 2$ cases. When the gap between the cylinders is increased, the steady streaming mechanism tends to pretend as it was in the single cylinder. When Figure 4.4, Figure 4.6 and Figure 4.9 are examined, it can be said that the scour and deposition patterns and the regions of them are similar to each other.

Figure 2.7 shows the vector diagram of period averaged velocities (steady streamings at three different distances from the bed, namely z=0.4 cm, 5 cm and 25 cm (Sumer and Fredsøe, 2001). And Figure 2.9 shows the contour plot of bed topography in equilibrium stage for live bed condition. In this study, the period averaged velocities were not measured. In this study, period averaged velocities were not measured. However, when the Figure 2.7 and Figure 4.4 (a) compared, it is possible to say that the velocities in region B for both studies have similar characteristics. When figure 2.9 and Figure 4.5 (b) were compared, it was seen that there were scour generation both in these regions. However, region A and region C are different for these two cases. it is because of the different boundary conditions.

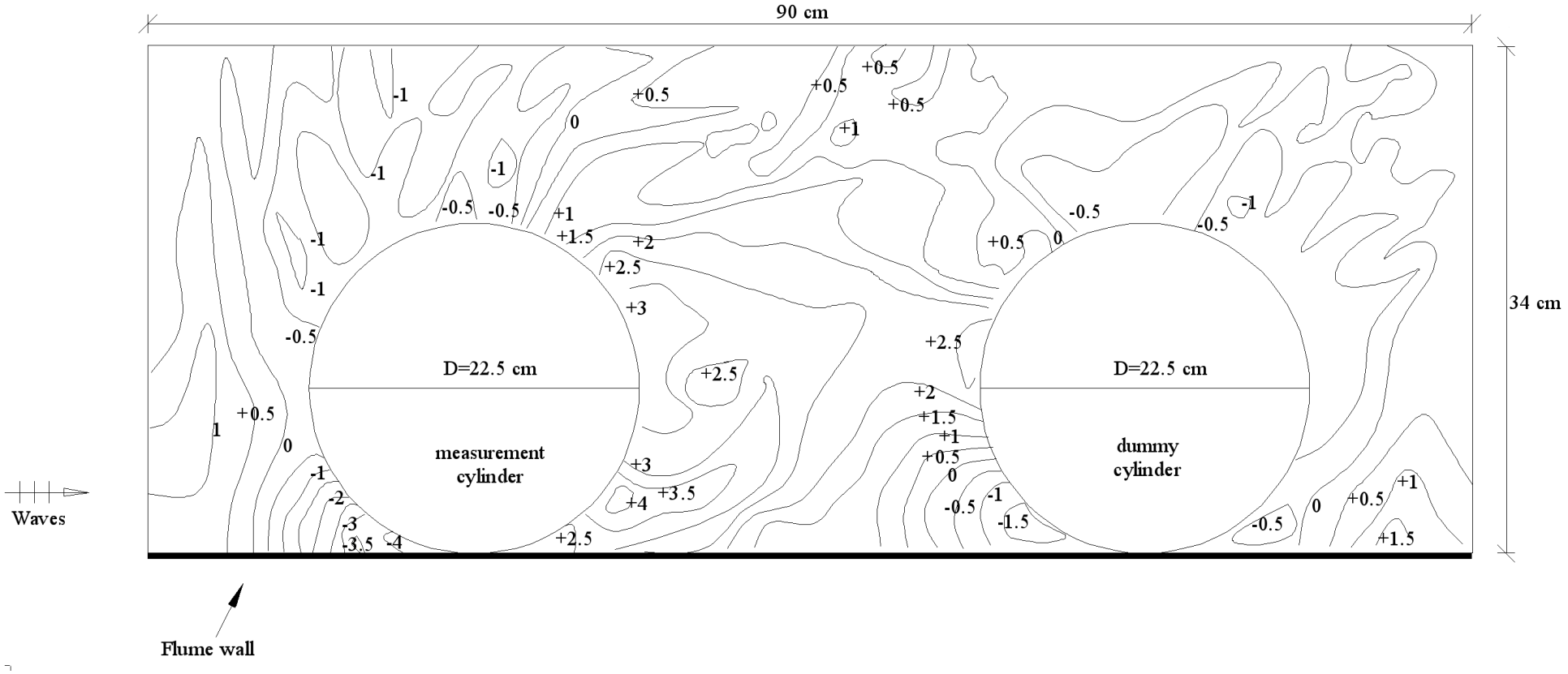

Figure 4.8 : For $x/D = 2$ (measurement cylinder is at the incoming wave side) and live bed, contour lines for the final bed topography (Scour and depositions are in cm).

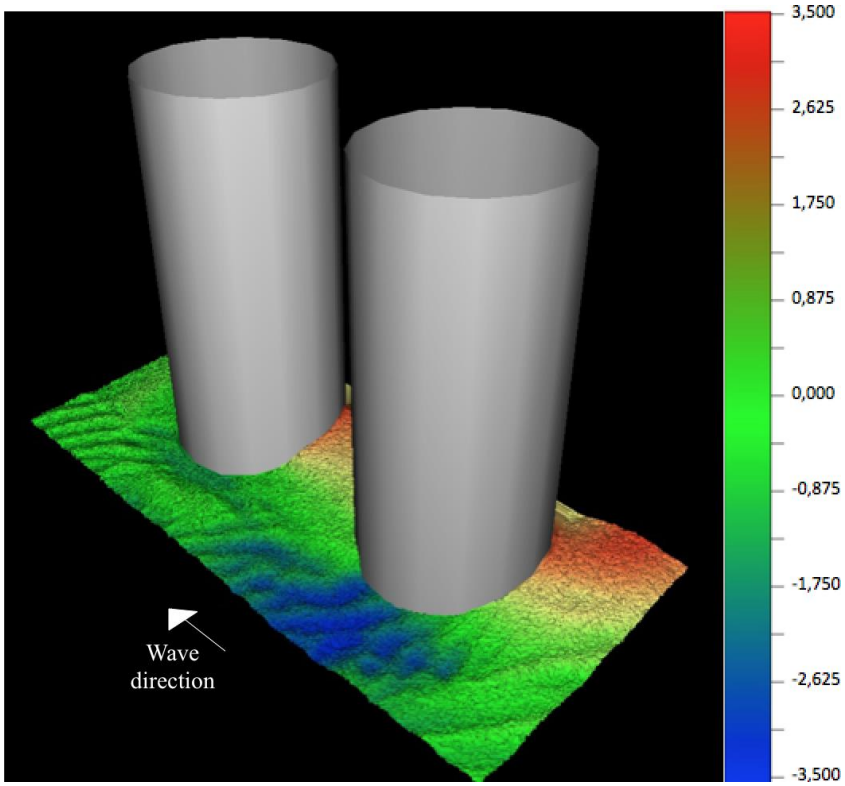

(a)

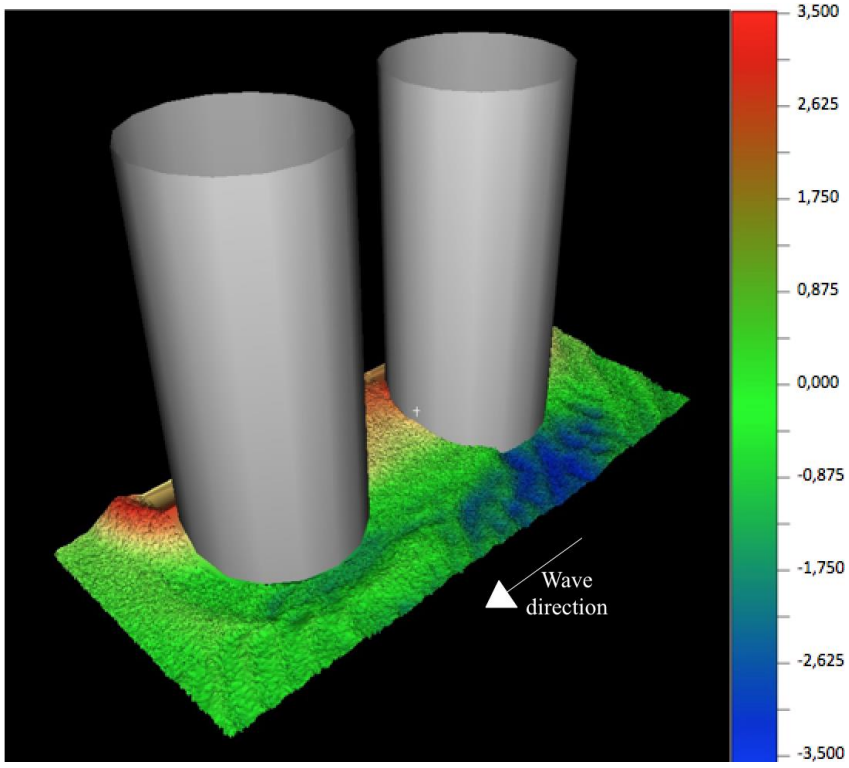

(b)

Figure 4.9 : The scour and deposition pattern around the cylinder for $x/D = 1.5$ (measurement cylinder is at the incoming wave side), live bed, a) incoming wave side, b) sheltered side (The legend values are in cm).

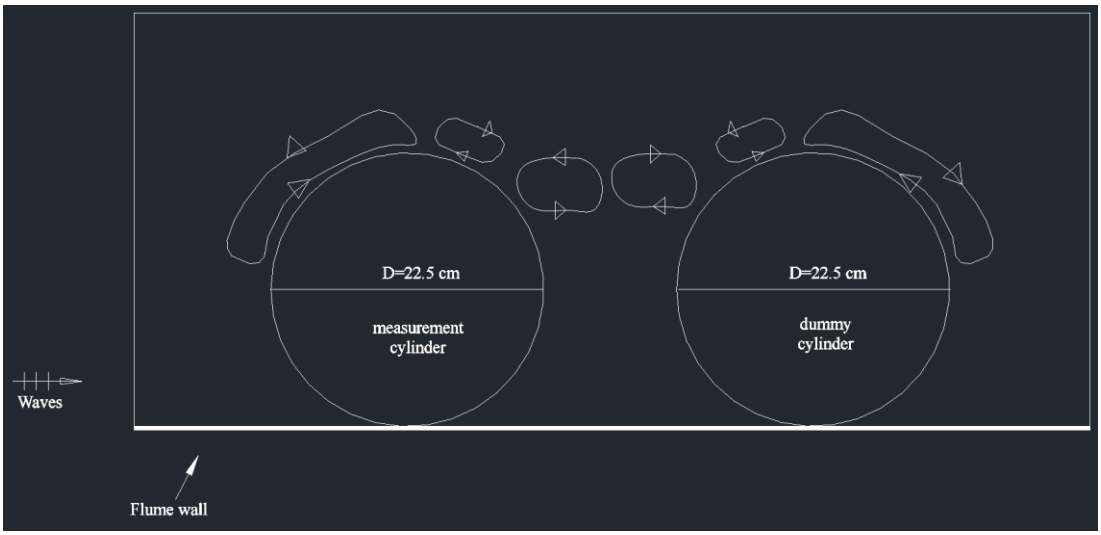

(a)

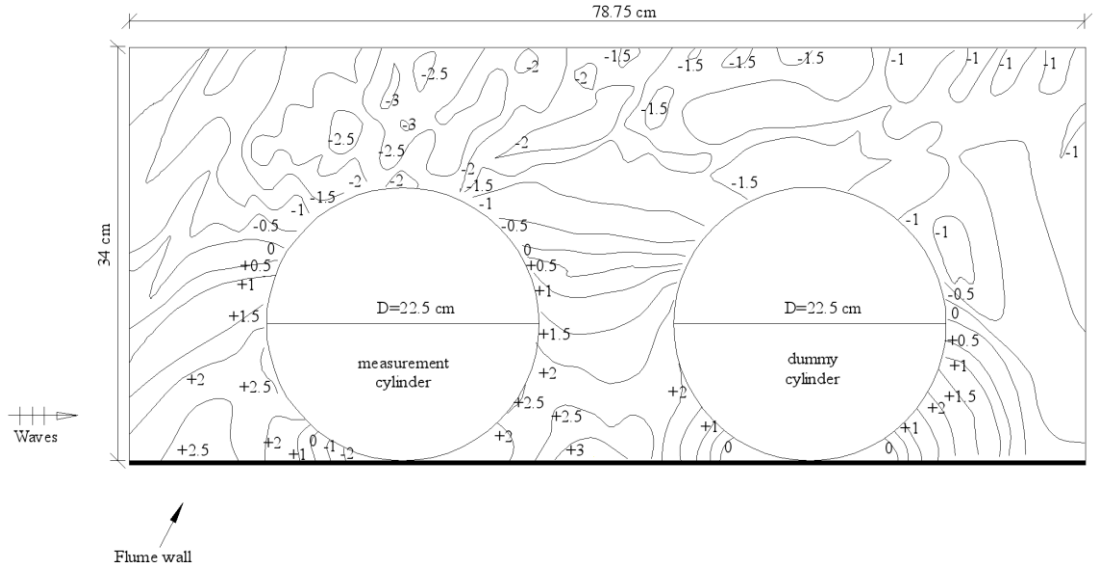

(b)

Figure 4.10 : For x/D=1.5 (measurement cylinder is at the incoming wave side) and live bed, a) definition sketch of streaming around the cylinder, b) contour lines for the final bed topography (Scour and depositions are in cm).

Figure 4.5 (a), Figure 4.7 and Figure 4.10 (a) indicated that the streamings are symmetric due to the center point of the system. When Figure 4.7 and Figure 4.10 (a) are compared, it can be said that the streaming between the measurement and dummy cylinders was disappeared for $x/D = 2$. Since the gap between the cylinders is increased, the steady streaming mechanism tends to pretend as it was in the single cylinder. When Figure 4.4, Figure 4.6 and Figure 4.9 are examined, it can be said that the scour and deposition patterns and the regions of them are similar to each other.

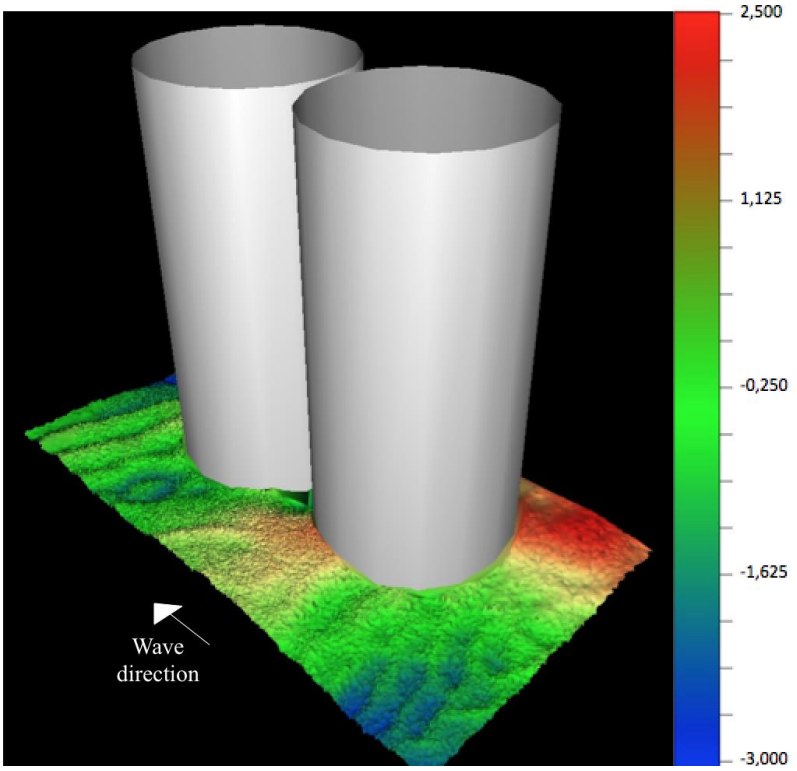

(a)

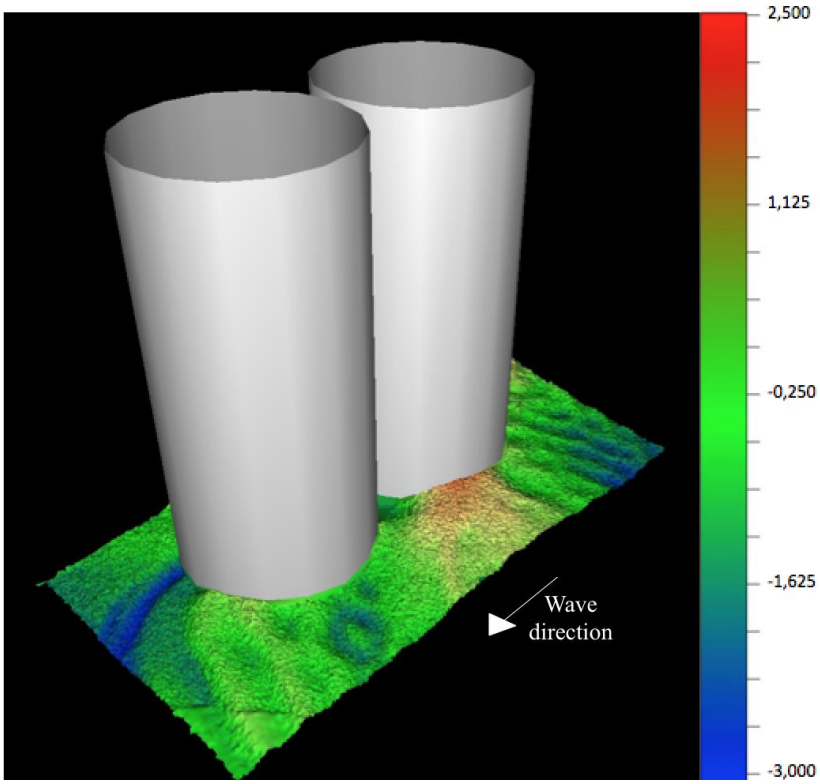

(b)

Figure 4.11 : The scour and deposition pattern around the cylinder for $x/D = 1$ (measurement cylinder is at the incoming wave side) and live bed, a) incoming wave side, b) sheltered side (The legend values are in cm).

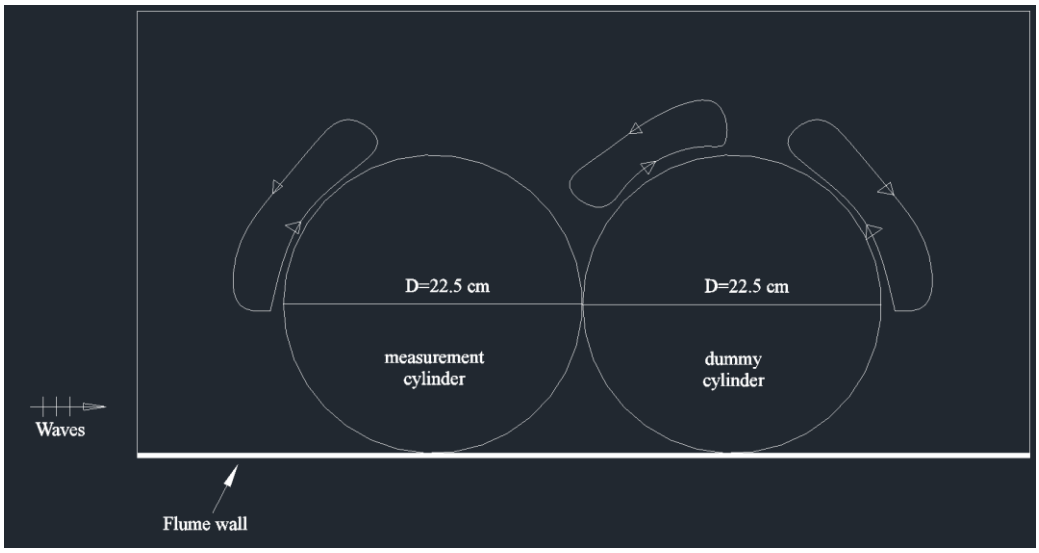

(a)

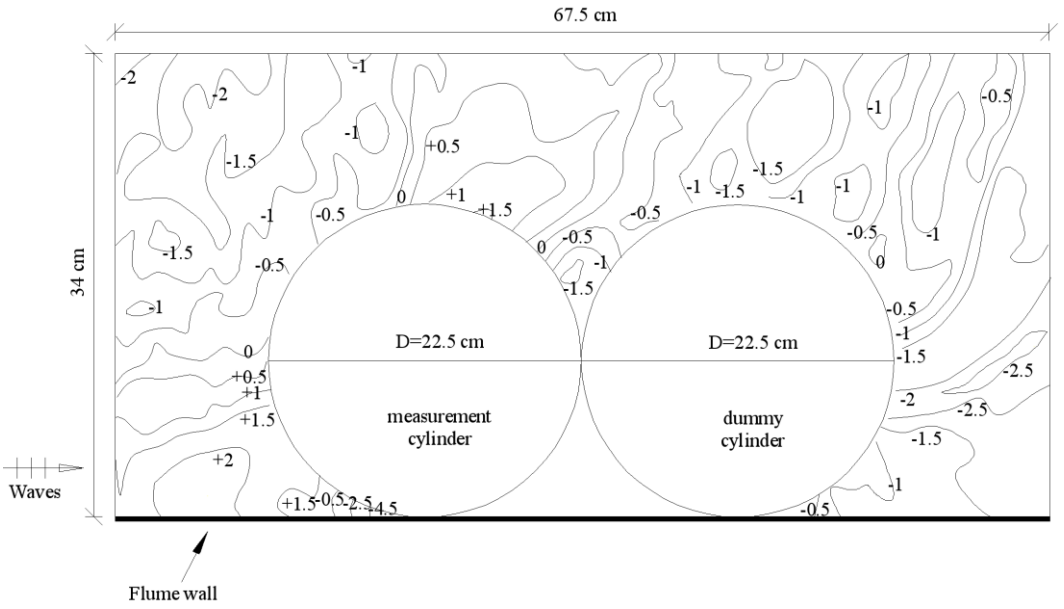

(b)

Figure 4.12 : For x/D=1 (measurement cylinder is at the incoming wave side) and live bed, a) definition sketch of streaming around the cylinder, b) contour lines for the final bed topography (Scour and depositions are in cm).

Figure 4.12 shows that in the region, which the experimental and dummy cylinders are attached to each other, a scour generation was observed. This scour is may be independent from the streaming induced scour. (The laser scanner could not scan the region between the two cylinders and the flume wall in Figure 4.12; therefore there are no contour lines).

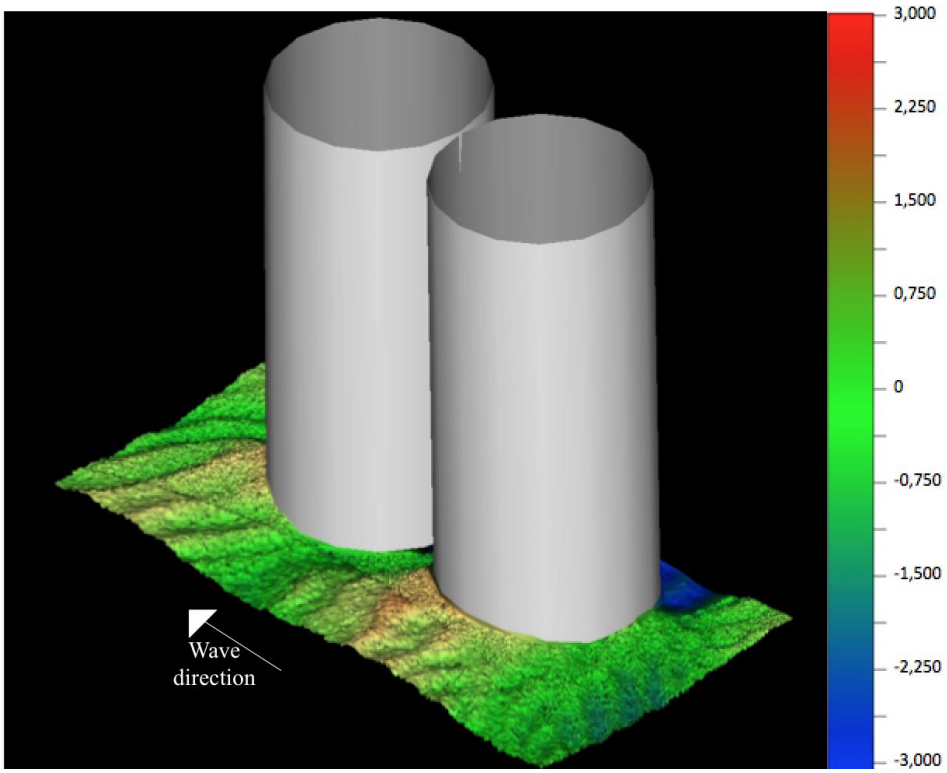

(a)

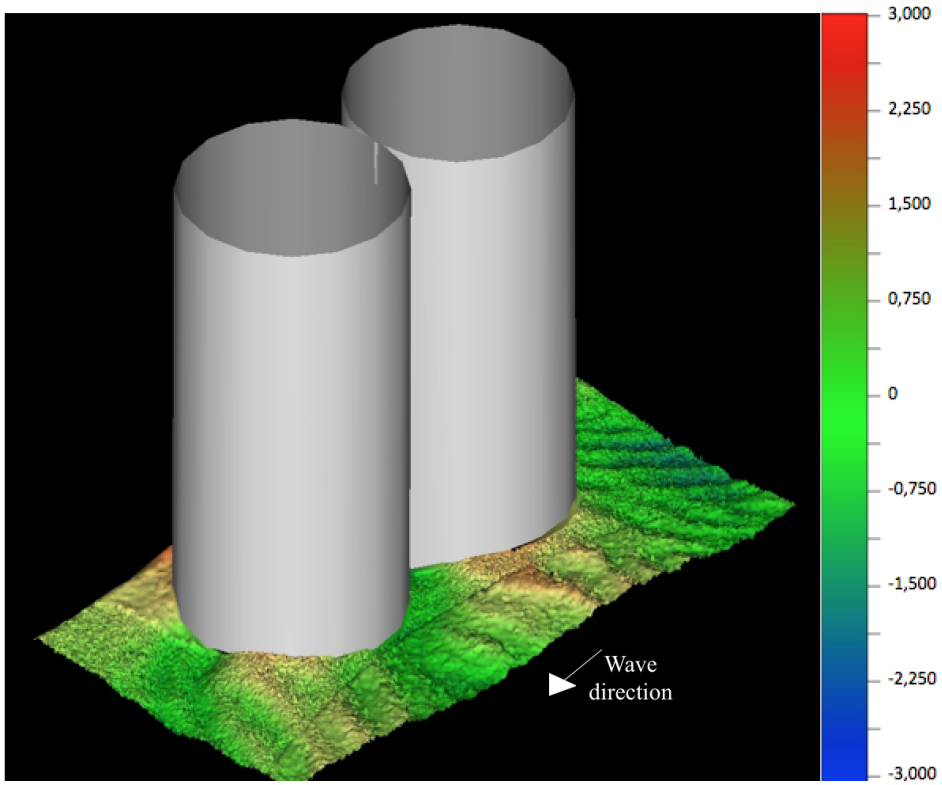

(b)

Figure 4.13 : The scour and deposition pattern around the cylinder for $x/D = 1$ (dummy cylinder is at the incoming wave side) and live bed, a) incoming wave side, b) sheltered side (The legend values are in cm).

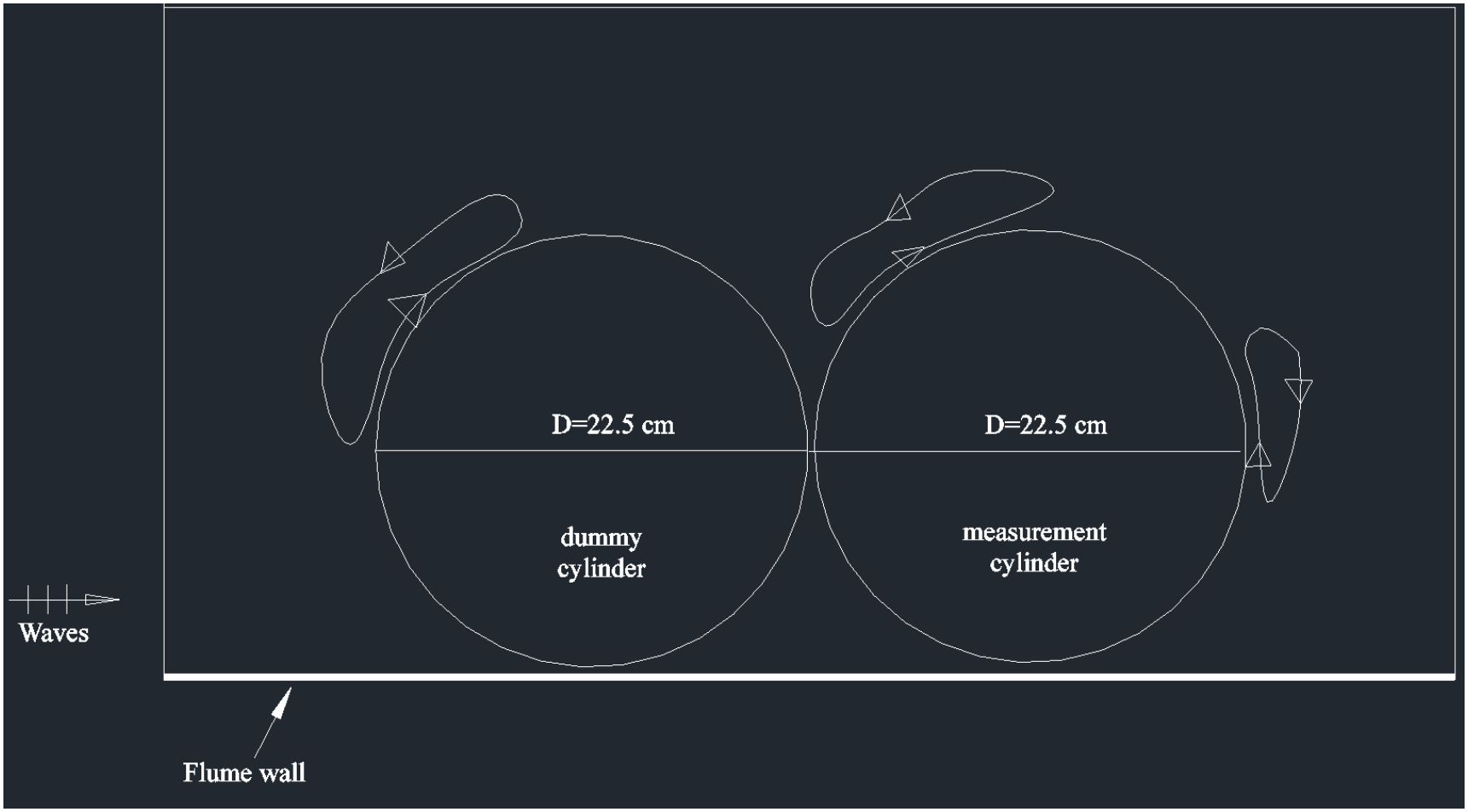

Figure 4.14 : For $x/D = 1$ (dummy cylinder is at the incoming wave side) and live bed, definition sketch of streaming around the cylinder.

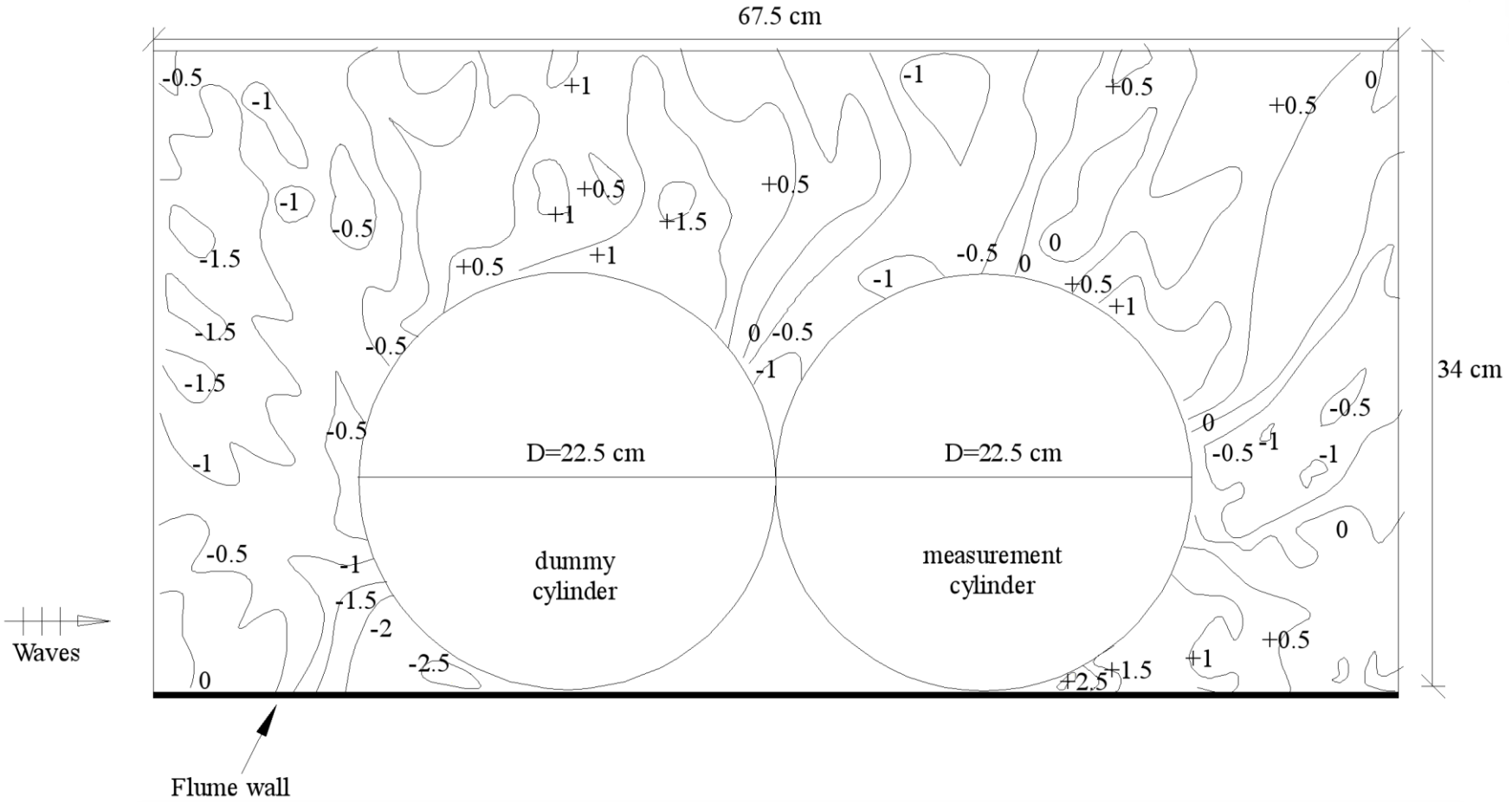

Figure 4.15 : For $x/D = 1$ (dummy cylinder is at the incoming wave side) and live bed, contour lines for the final bed topography (Scour and depositions are in cm).

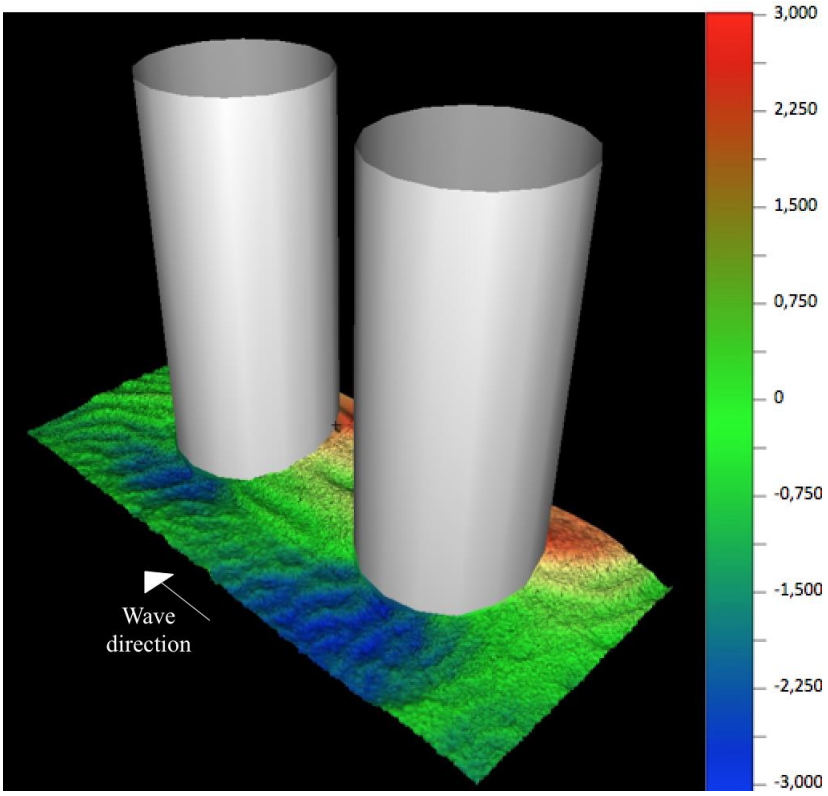

(a)

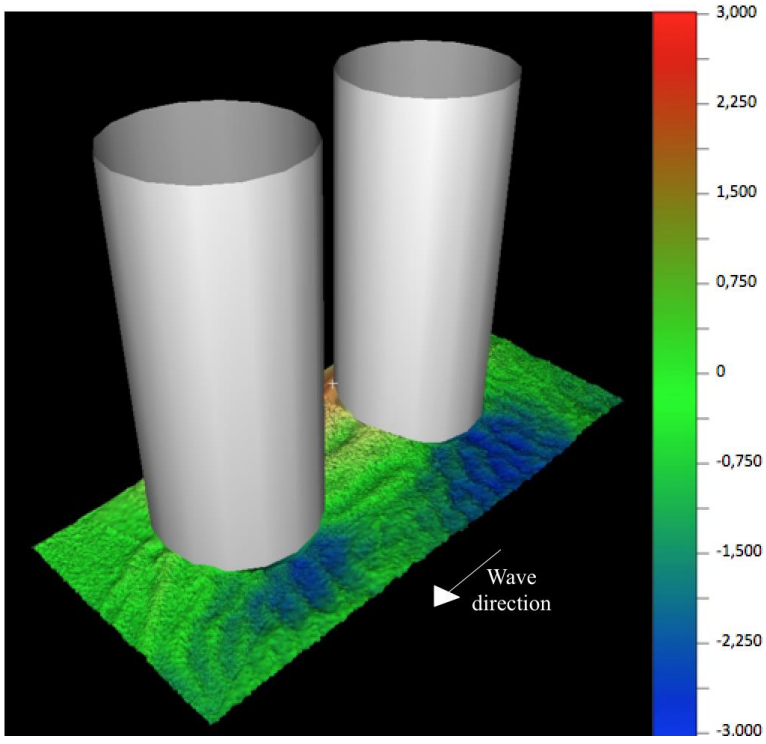

(b)

Figure 4.16 : The scour and deposition pattern around the cylinder for $x/D = 1.5$ (dummy cylinder is at the incoming wave side) and live bed, a) incoming wave side, b) sheltered side (The legend values are in cm).

According to Figure 4.4 (a), scour occurs in the region B. When all the figures related to streaming induced scour are examined, it can be indicated that scour occurs in region B in all the tests. And in the shadow zone for tandem cylinder cases, namely between the cylinders, deposition occurs. Since the sediment transported by the effect of the streaming from B towards this region caused a deposition. This process can be explained by steady streaming around the cylinders. And in the region 1 (Figure 4.4 (a)), deposition occurs. However, when the region between the cylinder and flume wall are investigated, there can be seen a scour hole for all the tests, as mentioned in the preceding paragraphs, in vortex induced scour.

According to the contour maps (Figure 4.5, Figure 4.8, Figure 4.10, Figure 4.12, Figure 4.15, Figure 4.18, Figure 4.20), it can be said that the maximum scour at the offshore side of the cylinder occurs for the cases where $x/D = 1.5$, while the minimum scour occurs in $x/D = 1$ and the mechanism of scour may be explained by steady streaming. The maximum scour depth in the steady streaming region was observed in the case of $x/D = 1.5$ cases and S/D was found approximately as 0.09~0.13. The minimum scour depth was observed in the case of $x/D = 1$.

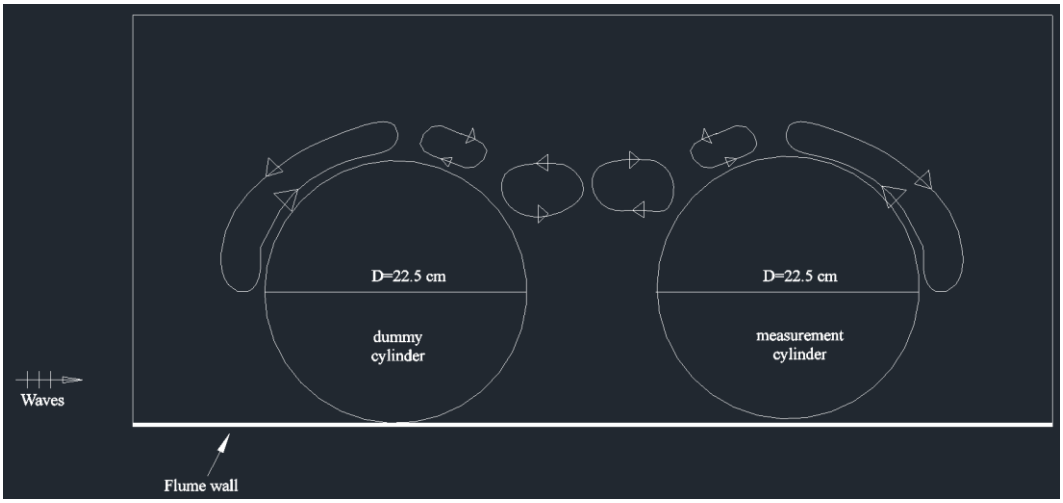

Figure 4.17 : For $x/D = 1.5$ (dummy cylinder is at the incoming wave side) and live bed, definition sketch of streaming around the cylinder.

Sumer and Fredsøe (2001) found the maximum scour depth to the cylinder diameter ratio, namely S/D=0.04 in their experimental study for KC=1.1 and D/L=0.15 and Khalfin (2007) indicated that the maximum S/D ratio was 0.08 for KC≅1. In present study, it was found as 0.09~0.13 for KC≅1. It may be said that the presence of the flume wall affects the scour depth around the cylinder.

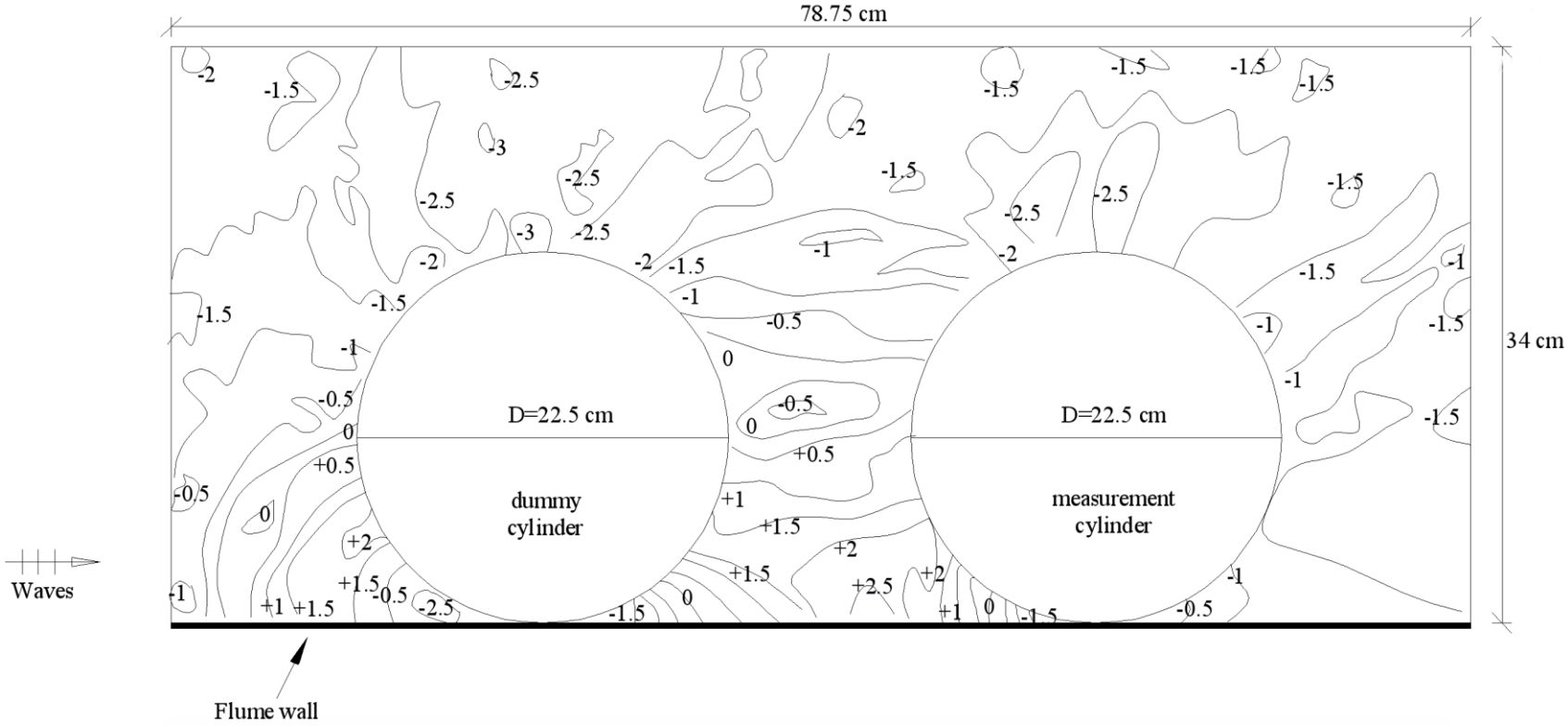

Figure 4.18 : For $x/D = 1.5$ (dummy cylinder is at the incoming wave side) and live bed, contour lines for the final bed topography (Scour and depositions are in cm).

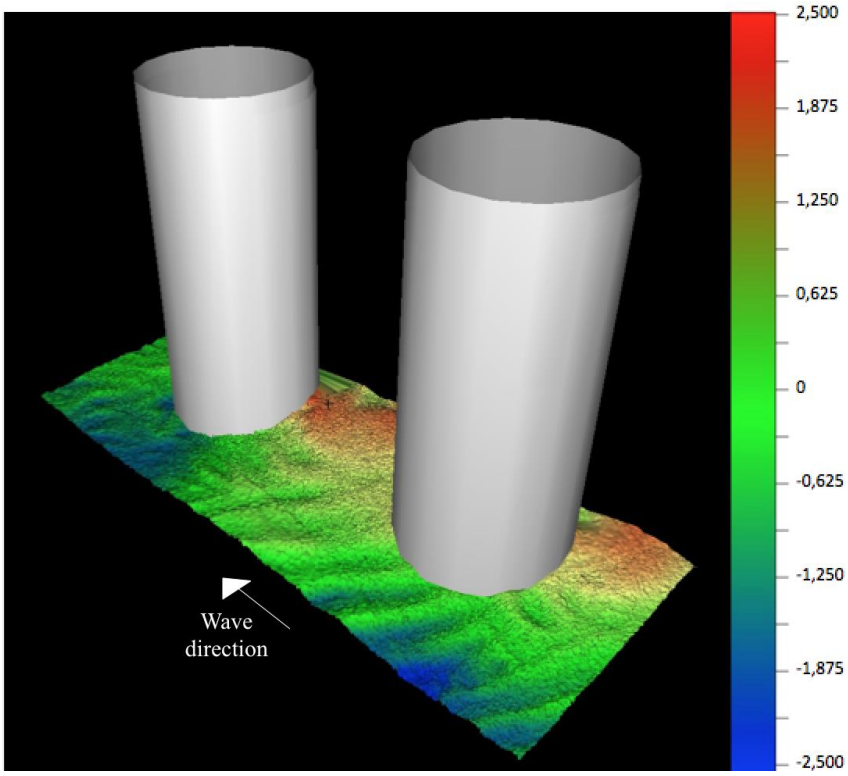

(a)

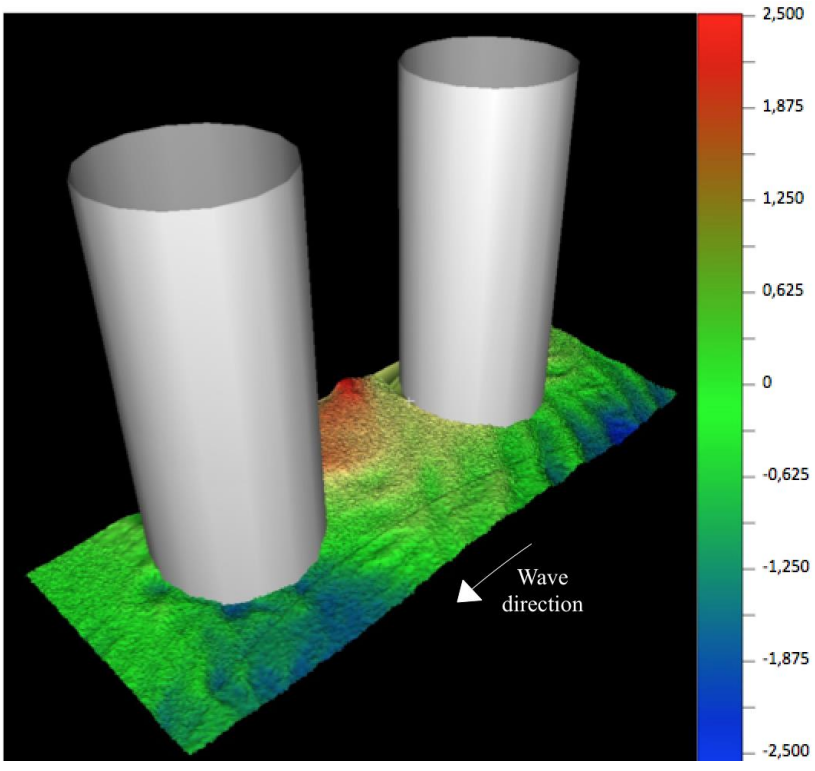

(b)

Figure 4.19 : The scour and deposition pattern around the cylinder for $x/D = 2$ (dummy cylinder is at the incoming wave side) and live bed, a) incoming wave side, b) sheltered side (The legend values are in cm).

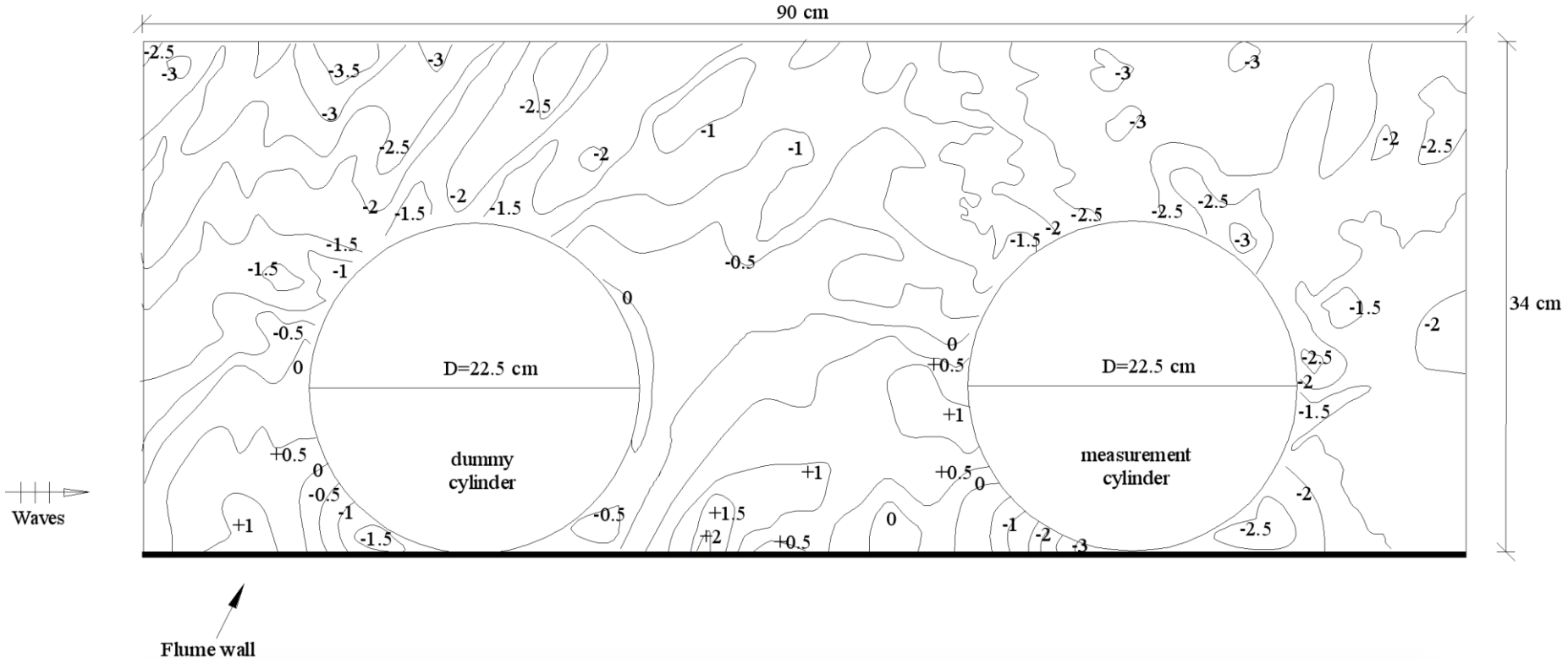

Figure 4.20 : For $x/D = 2$ (dummy cylinder is at the incoming wave side) and live bed, contour lines for the final bed topography (Scour and depositions are in cm).

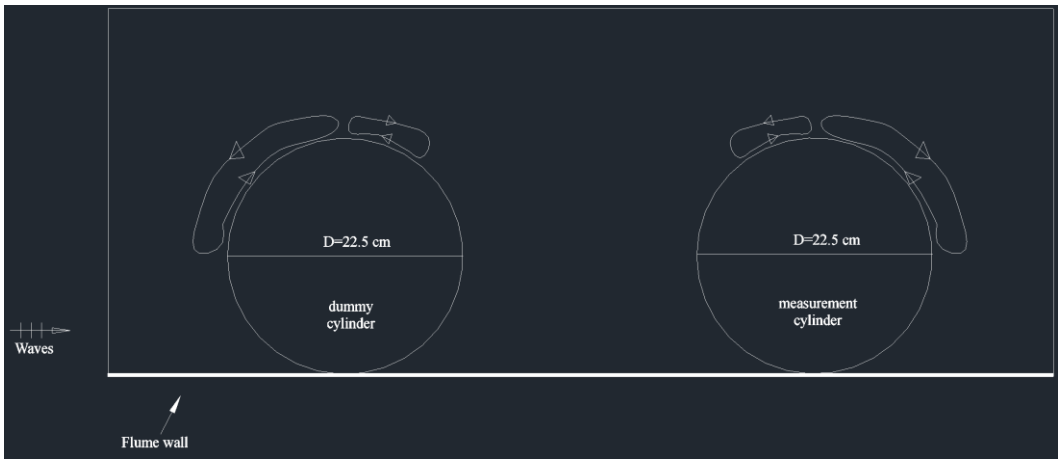

Figure 4.21 : For $x/D = 2$ (dummy cylinder is at the incoming wave side) and live bed, definition sketch of streaming around the cylinder.

For the region 2, which is shown in Figure 4.5 (b), the x/D versus S/D were drawn in a graph (Figure 4.22). According to Figure 4.22, the most negatory case is when $x/D = 1.5$. From this figure, it can be said that the minimum scour depth in this region was observed for the $x/D = 1$ cases. The single cylinder and $x/D = 2$ cases gives approximate results in this region. Therefore, it may be said that when the gap between the cylinders is increased, the system began to behave as a single cylinder.

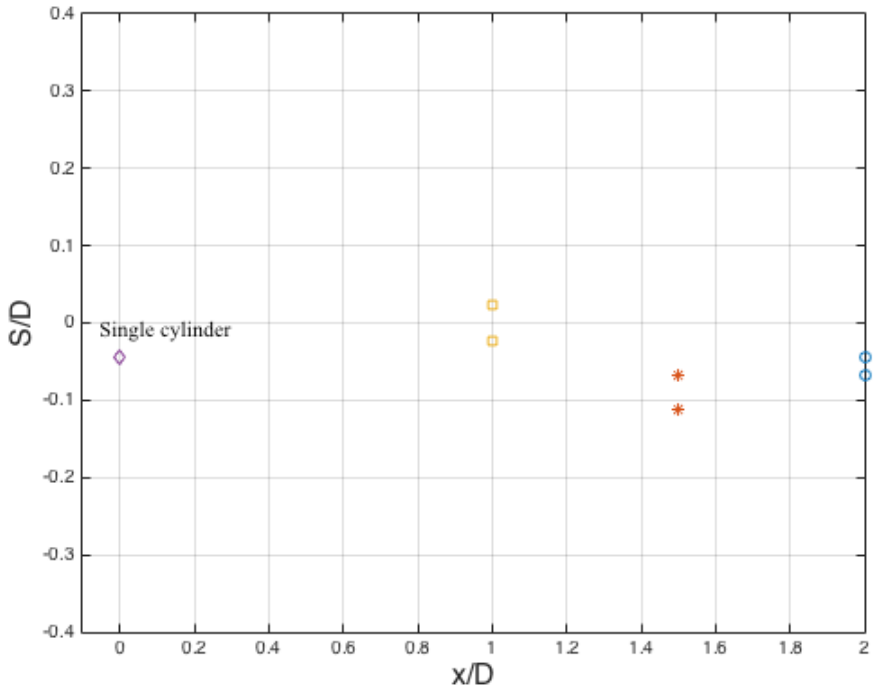

Figure 4.22 : The change in scour depth versus the gap between the cylinders.

4.2 Pressure Distributions and Forces Around the Cylinder

Pressure measurements were made with the pressure transducers at 5 different points which are located 45° interval at a horizontal plane, which was 5 cm above the bed (Figure 4.23).

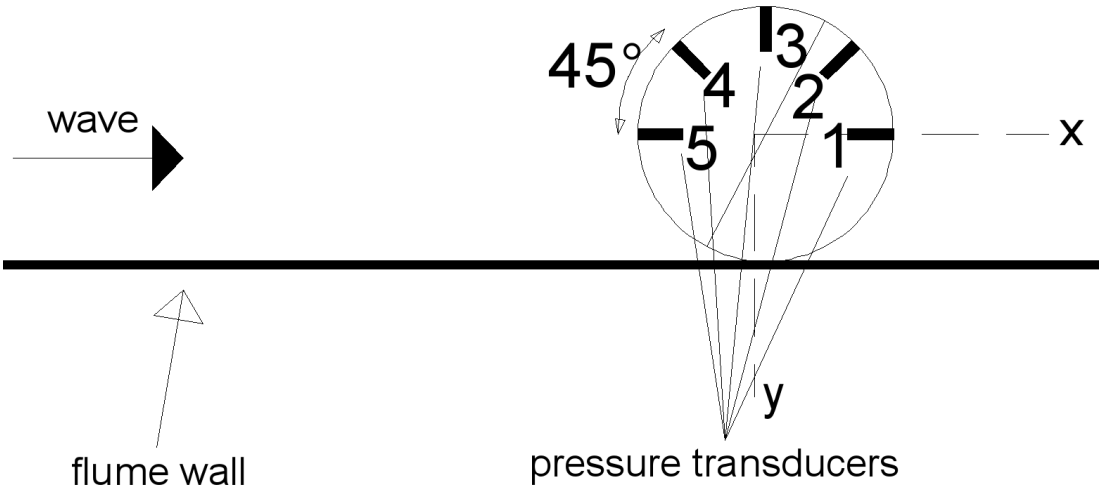

Figure 4.23 : Plan view of the pressure transducers on the surface of the cylinder above 5 cm from the bed.

The pressure values in rigid bed experiments for single cylinder and tandem cylinder cases were found dimensionless with a pressure coefficient by using the equation 4.1 (Cokgor and Avci, 2002) and given in the Figure 4.24.

$$c_p = \frac{p - p_0}{\frac{1}{2}\rho U_m^2} \tag{4.1}$$

Herein, p and p_0 represent the measured pressure and the hydrostatic pressure, respectively.

When the dummy cylinder was replaced at the incoming wave side, the pressure coefficient, c_p takes smaller values than it was in the sheltered side of the measurement cylinder, as can be seen from Figure 4.24. Because the dummy cylinder is an obstacle in front of the measurement cylinder. The pressure coefficient values were pretty much the same in the cases of single cylinder and $x/D = 2$ cases. Hence, it can be indicated that when the gap between the cylinders exceeds 2, the system can be considered as a single cylinder case.

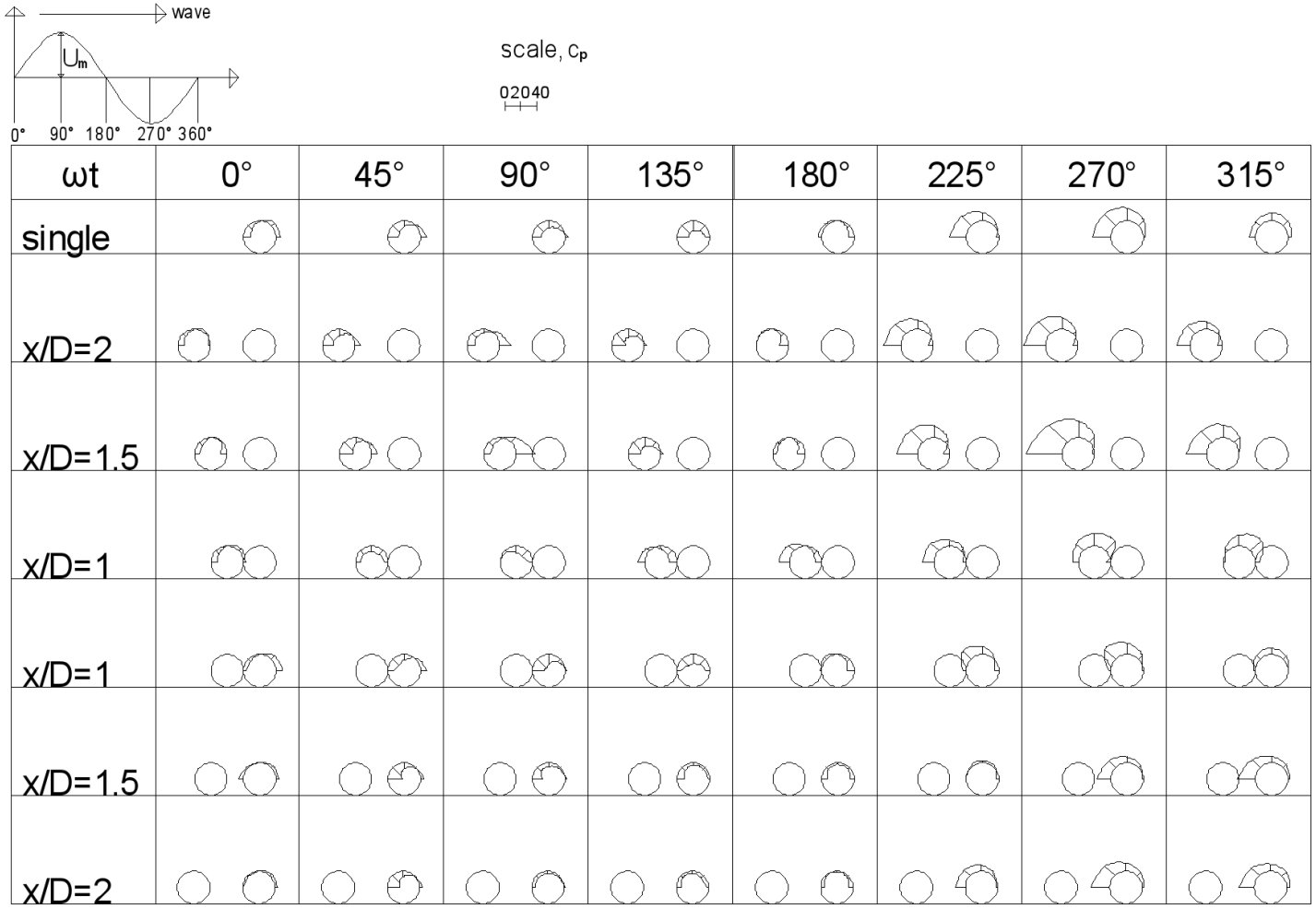

Figure 4.24 : Instantaneous pressure distribution during one cycle of wave in rigid bed experiments for single cylinder and tandem cylinder cases, $KC = 0.74$.

From the Figure 4.24, it can be said that the magnitude of pressure that was measured before the wave reversed ($\omega t = 180°$) are almost same with the pressure, which measured after the wave reversed. Another important issue that can be written is about the largest c_p values. The maximum c_p values are obtained at the fifth pressure measurement point (Figure 4.23). Since in this point, the reflected wave and the incoming wave are combined and pressure values are increased, when the dummy cylinder is at the sheltered side of the measurement cylinder. However, when the dummy cylinder is at the incoming wave side, this situation was observed again. This is due to the increment of hydrodynamic forces caused by the interaction of cylinders and flow in this region. From the Figure 4.24, it can be said that maximum pressure values were observed in the $x/D = 1.5$ cases and the minimum values of pressures were seen in $x/D = 1$ cases.

In the Figure 4.25, the 5 seconds of pressure distribution on the measurement point 5 is given. This figure shows that there is a pressure decrement with time, namely the largest values were measured at the initial state, and while the smallest pressure values were obtained in the final state.

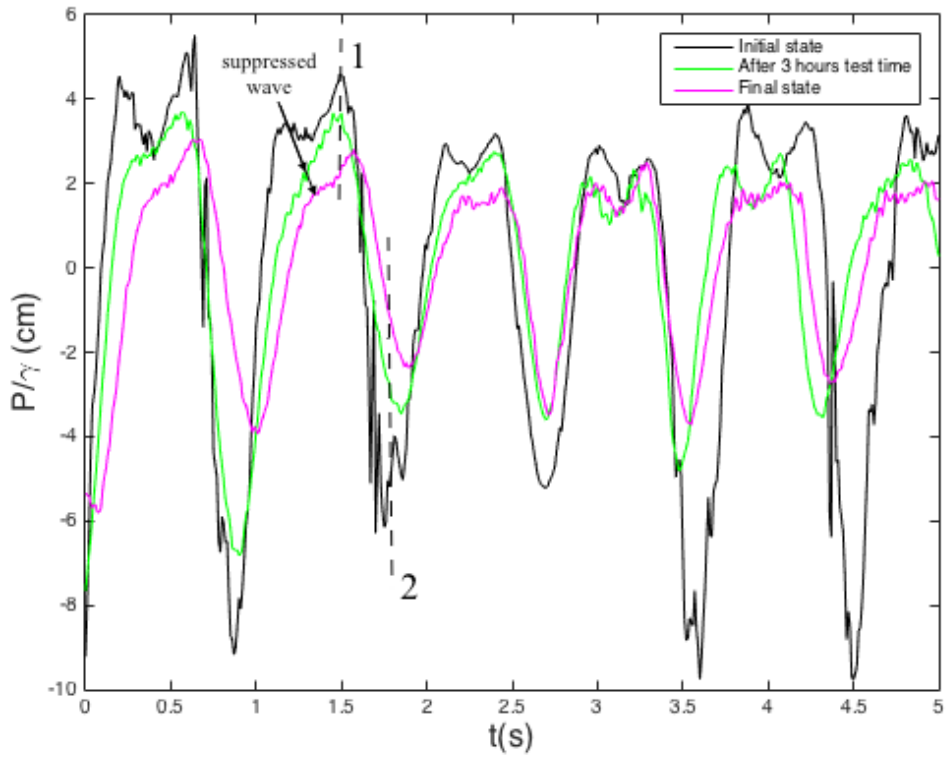

Figure 4.25 : Pressure distribution at the measurement point 5 in single cylinder case for initial state, after 3 hours test time and final state of the test.

In all the experiments, the scour process in front of the fifth pressure measurement section was taped. When the recorded scour and depositions and measured pressures given in the Figure 4.25 were evaluated together, it was seen that when deposition occurs, the pressure was suppressed (Figure 4.26). Figure 4.26 shows the relative distance between the bed levels at the pressure section 1 and section 2 showed in the Figure 4.25.

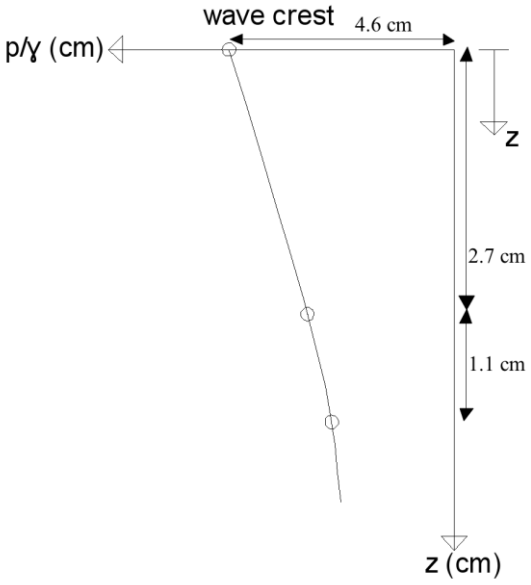

(a)

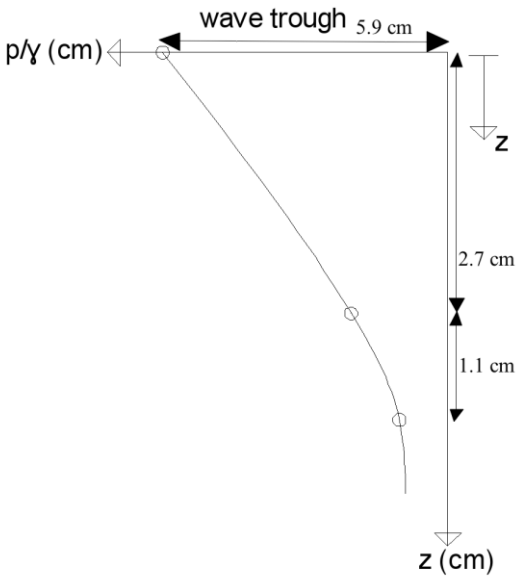

(b)

Figure 4.26 : The bottom level and pressure relation at the wave crest and wave trough a) section 1 given in Figure 4.24, b) section 2 given in Figure 4.24, where z shows the deposition.

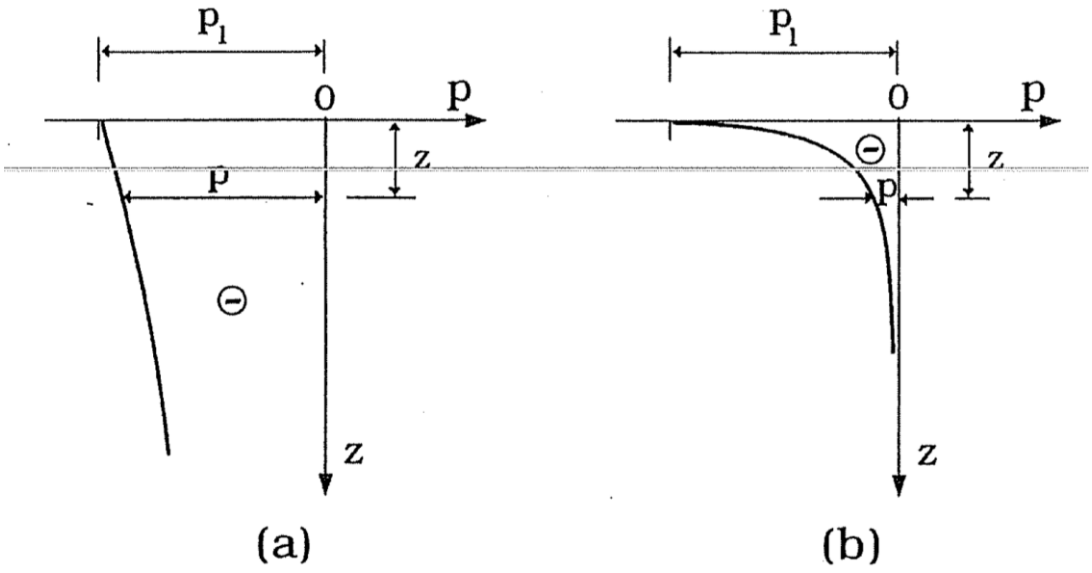

Figure 4.27 : Typical distributions os pore pressure (in excess of hydrostatic pressure) during the passage of wave trough (a) saturated soil, (b) unsaturated soil (Sumer and Fredsøe, 2002).

When Figure 4.26 and Figure 4.27 are compared, it can be seen that the findings shown in figure 4.26 coincides with the study of Sumer and Fredsøe's (2002).

The in-line forces acting on the unit height of the cylinder was calculated by using equation 2.4. In this study, the pressure transducers were located on the half of the measurement cylinder, as shown in Figure 4.23. When the forces acting on the surface on the cylinder was calculated, an interpolation was made for the other half of the cylinder (Figure 4.28). In Figure 4.28, the pressure of the point a was considered as it equals to the pressure measured at the fifth pressure channel. Pressure at point b is zero, due to the presence of wall. Pressure value at c point was taken as the half of the pressure, which was measured at the first channel.

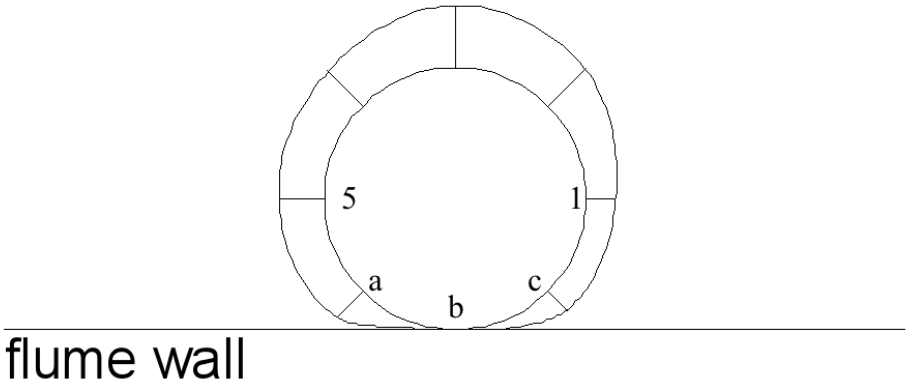

Figure 4.28 : Interpolation sketch.

The calculated forces were made dimensionless by using the following equation:

$$\frac{F_x}{\frac{1}{2}\rho D U_m^2}, \qquad \frac{F_y}{\frac{1}{2}\rho D U_m^2} \tag{4.2}$$

The positive directions of the F_x and F_y forces were given in Figure 4.23. The in-line forces are given in the Figure 4.29 for single cylinder case.

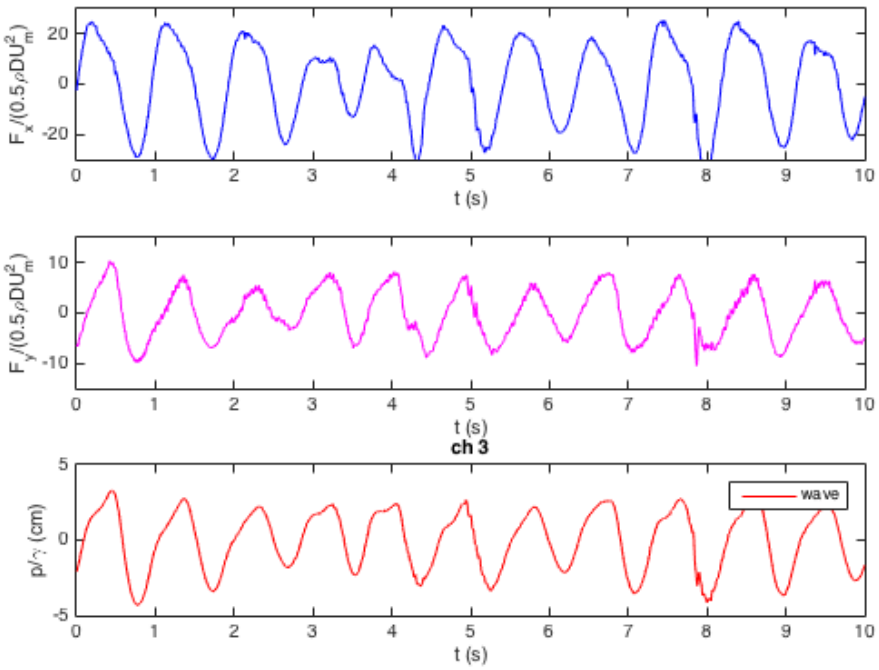

Figure 4.29 : The dimensionless in-line forces acting on the surface of the measurement cylinder for single cylinder case.

5. CONCLUSION AND RECOMMENDATIONS

Scour and flow around piles and piles-sheet piles combination wharf structures were investigated in the present study experimentally. Results and recommendations about further work could be given as follows:

- Scour around the pile supported wharf structures become a significant issue under waves.
- In all the experiments, a vortex mechanism was observed, which may be indicated, as it is similar to horseshoe vortex between the cylinder and sheet pile in spite of low KC number.
- Steady streaming is an important flow structure around the cylinder.
- Streaming zones are versatile around the cylinder which depending on the boundary conditions such as single cylinder or another cylinder around the mentioned one.
- In the single cylinder experiment, vortex based scour was observed between sheet pile and flume wall at the incoming wave side and steady streaming forced scour was observed offshore side of the cylinder (Figure 4.4). The maximum scour depth was reached as $S/D = 0.18$ in the vortex region and $S/D = 0.08$ in the steady streaming zone. Deposition was determined between vortex and steady streaming regions and the maximum deposition height was measured as $0.11D$.
- In the tandem cylinder case, scour was always observed between the flume wall and cylinder as well as single cylinder case because of horseshoe vortex forcing. Streaming zone(s) were changing in size, in numbers and in strength with the boundary conditions, namely with the different x/D ratios. Scour depth and placement also follows these variations.
- The maximum scour depth was observed in the $x/D = 1.5$ cases as $S/D = 0.09 \sim 0.13$.

- When the x/D ratio reaches to 2, flow around the cylinders close to single cylinder case and scour phenomena follows that flow condition. The pressure measurements support this idea.
- Pressure distribution around the cylinder was close to the marine pipeline experiments case (Cokgor and Avci, 2002), besides in vortex zone, in this region, pressure accumulation during the wave crest was observed then this accumulation had released immediately during the wave trough.
- The results pointed out, in $x/D = 1.5$ cases, the scour reaches its maximum value. This case may be a threat to the structural stability. Therefore, this condition in structural design must be avoided.

REFERENCES

An, H., Cheng, L., Zhao, M., (2009). Steady streaming around a circular cylinder in oscillatory flow. *Ocean Engineering, 36(14), 1089-1097*

Briaud, J. L., Ting, F. C., Chen, H.C., Gudavalli, R, Perugu, S. Wei, G. (1999). SRICOS: Prediction of scour rate in cohesive soils at bridge piers. *Journal of Geotechnical and Geoenvironmental Engineering, 125*(4), 237-246

Cokgor, S., Avcı, I. (2002). Hydrodynamic forces on a partly buried cylinder exposed to combined waves and current. *Ocean engineering, 29*(7), 753-768.

Fredsϕe, J. and Deigaard, R. (1992). *Mechanics of Coastal Sediment Transport* Vol. 3. World Scientific.

Holthuijsen, L. H. (2010). *Waves in Oceanic and Coastal Waters.* Cambridge University Press.

Isaacson, M. (1979). Wave-induced forces in the diffraction regime. *Mechanics of Wave-Induced Forces on Cylinders*, 68-89.

Kamphuis, J. W. (1975). Friction factor under oscillatory waves. *Journal of the Waterways Harbors and Coastal Engineering Division, 101*(2), 135-144.

Katsui, H. and Toue, T. (1988). Inception of sand motion around a large obstacle. *Coastal Engineering Proceedings, 1*(21), 41-53.

Katsui, H., & Toue, T. (1993). Methodology of estimation of scouring around large-scale offshore structures. *In The Third International Offshore and Polar Engineering Conference*, International Society of Offshore and Polar Engineers.

Khalfin, I. S. (2007). Modeling and calculation of bed score around large-diameter vertical cylinder under wave action. *Water Resources*, *34*(1), 49-59.

National bridge inventory. (1997). Bridge Management Branch, Federal Highway Administration, Washington, D.C.

Nortek AS. (2004). Vectrino User Guide. Norway.

Qi, W. G., & Gao, F. P. (2014). Physical modeling of local scour development around a large-diameter monopile in combined waves and current. *Coastal Engineering*, *83*, 72-81.

Rance, P. J. (1980). The potential for scour around large objects. *Scour Prevention Techniques Around Offshore Structures*, 41-53.

Schlichting, H. (1979). *Boundary-Layer Theory*, 7th Ed., McGraw-Hill, New York.

Sumer, B. M., Christiansen, N., (1992). Scour around vertical pile in waves. *Journal of Waterway, Port, Coastal, and Ocean Engineering, 118*(1), 15-31.

Sumer, B. M. and Fredsϕe, J. (1997). *Hydrodynamics Around Cylindrical Structures*. Vol. 12. World Scientific.

Sumer, B. M. and Fredsϕe, J. (2001). Wave scour around a large vertical circular cylinder. *Journal of Waterway, Port, Coastal, and Ocean Engineering, 127*(3), 125-134

Sumer, B. M. and Fredsϕe, J. (2002). *The Mechanics of Scour In The Marine Environment.* World Scientific.

Sumer, B. M., Whitehouse, R. J., Tørum, A. (2001). Scour around coastal structures: a summary of recent research. *Coastal Engineering, 44*(2), 153-190.

Sumer, B. M. (2007). Mathematical modelling of scour: A review. *Journal of Hydraulic Research, 45*(6), 723-735.

Sumer, B. M. (2013). Lecture notes on turbulence.

Umeda, S. (2011). Scour regime and scour depth around a pile in waves. *Journal of Coastal Research,* (64), 845.

Zanke, U. C., Hsu, T. W., Roland, A., Link, O., & Diab, R. (2011). Equilibrium scour depths around piles in noncohesive sediments under currents and waves. *Coastal Engineering*, *58*(10), 986-991.

Url-1 <*http:// www.mesens.com/en/*>, date retrieved 18.04.2016

Url-2 < http://*www.teknikdestek.com.tr/en/*>, date retrieved 18.04.2016.

Url-3 <*http://* hds.leica-geosystems.com/en/>, date retrieved 19.04.2016.

CURRICULUM VITAE

Name Surname **: Dila Demiral**

Place and Date of Birth **: Kocaeli / 17.04.1991**

E-Mail **: demiraldila@itu.edu.tr**

EDUCATION:

- **B.Sc.:** 2014, İstanbul Technical University, Civil Engineering Faculty, Civil Engineering Department
- **M.Sc.:** 2016, İstanbul Technical University, Civil Engineering Faculty, Hydraulics and Water Resources Engineering Programme

PROFESSIONAL EXPERIENCE:

- **2016-:** Research Assistant at İstanbul Technical University, Civil Engineering Faculty, Division of Hydraulics